



國立中山大學機械與機電工程學系

碩士論文

Department of Mechanical & Electro-Mechanical Engineering
National Sun Yat-Sen University
Master Thesis

跑步機正向與背向行走對腦波的影響

The Effect of Treadmill Forward and Backward Walking on
Electroencephalography Rhythms

研究生：黃瀛緯

Jung-Wei Huang

指導教授：嚴成文 博士

Dr. Chen-Wen Yen

中華民國 104 年 7 月

July 2015



國立中山大學機械與機電工程學系

碩士論文

Department of Mechanical & Electro-Mechanical Engineering
National Sun Yat-Sen University
Master Thesis

跑步機正向與背向行走對腦波的影響

The Effect of Treadmill Forward and Backward Walking on
Electroencephalography Rhythms

研究生：黃瀛緯

Jung-Wei Huang

指導教授：嚴成文 博士

Dr. Chen-Wen Yen

中華民國 104 年 7 月

July 2015

國立中山大學研究生學位論文審定書

本校機械與機電工程學系碩士班

研究生黃融緯（學號：M013020113）所提論文

跑步機正向與背向行走對腦波的影響

The effect of treadmill forward and backward walking on
electroencephalography rhythms

於中華民國 104 年 6 月 29 日經本委員會審查並舉行口試，
符合碩士學位論文標準。

學位考試委員簽章：

召集人 陳沛仲 陳沛仲 委員 嚴成文 嚴成文

委員 李建德 李建德 委員 _____

委員 _____ 委員 _____

指導教授(嚴成文) 嚴成文 (簽名)

誌謝

這本碩士論文的完成，首先要感謝我的指導教授 嚴成文老師。這兩年在老師的悉心指導下，學習到許多專業上的知識與應用，填補了我專業能力上的空缺。尤其是老師願意讓我使用英文撰寫碩士論文，並不辭辛勞的幫我修改論文中的錯誤，更可以感受到老師對於教學除了擁有超人的熱情之外，還擁有過人的膽識。

感謝口試委員陳沛仲老師與李建德老師，於口試時給予的建議，使我的論文更加完整。

感謝於廣州中山大學交換學習時的指導教授宋嶸老師以及實驗室同學。於交換期間除了知識的學習之外，文化的交流也開闊了我的視野。

博士班學長志遠、柏霖、南宏與加力，碩士班已經畢業的同學懿軒、張浩、蔚蒲、奕廷、元輝、盈綺，一起畢業的誌良、俊瀚、國棟、敏棻，還沒畢業的學弟家瑋、博凱、銘宏、佳鴻，感謝你們在研究上的互相幫忙與協助，以及為實驗室所帶來的歡樂。

最後感謝我的家人與女友。在我決定離職，重拾書本準備研究所考試期間給予我的鼓勵與支持，並一起分擔我在求學期間的壓力。期望自己在畢業之後，仍然可以對學習充滿期待，對工作充滿熱情，並保有追逐理想的勇氣！

摘要

近年研究指出，中風患者於接受跑步機行走訓練後可以改善行走能力；而接受額外背向行走訓練的中風患者在行走能力、平衡能力上更具有正面療效。中風患者則是因大腦功能受損造成行動不便，而人類行走的機制與大腦皮質的活動又具有密切相關。故期望能藉由腦電圖訊號來觀察正向與背向行走對大腦皮質活動的影響，為行走復健訓練提供更多的生理資訊。

由於腦電圖的訊號非常微弱，極易受到外界訊號的干擾。若要建造良好的量測環境則會因量測成本較高使得普及化困難。本文使用一般商用跑步機以及量測電路作為地面反作用力與腦電圖的量測工具，藉由適應性濾波器消除行走所產生的行走干擾波，並利用獨立成分分析消除如心電圖、眼動圖、肌電圖等干擾訊號。最後再利用統計分析的方法，如峰值、峰態、頻譜能量等特徵來移除受雜訊汙染的腦電訊號。

行走中的腦電訊號增加適應性濾波器濾波後， $1.5\text{--}8.5\text{Hz}$ 的頻帶能量與行走干擾波的諧波能量均有顯著下降($p\text{-value}<0.05$)。將濾波後的腦電圖依照 σ 、 α 、 β 等腦波頻帶計算各別的腦波能量以及對稱性，藉由假設分析檢定來判別正向與背向行走的腦波是否具有差異。 α 波能量於正向行走後，在 F3、P3、P4、O1、O2 具有顯著減少($p\text{-value}<0.05$)；於背向行走後，在 F4、C3、C4、P3、P4 具有顯著減少($p\text{-value}<0.05$)；於背向行走時，在 C3、C4 頻道的 α_2 與 σ 能量顯著低於正向行走($p\text{-value}<0.05$)。

透過訊號處理以及統計分析的方法可以發現，正向行走與背向行走在不同頻道的 α 波與 β 波能量變化具有明顯差異。未來可利用此方法進一步改良與發展復健所需的生理指標與腦機介面。

關鍵字：跑步機、腦電圖、獨立成分分析、行走干擾波、適應性濾波器

Abstract

A recent study indicated that chronic stroke patient's balance ability and gait performance could be improved by additional backward walking training. Due to the locomotive ability and cerebral cortex activity are closely related, this study measured the electroencephalograph (EEG) to assess the effect of backward and forward walking on cortical activities.

However, the signal strength of EEG is too weak to prevent signal contamination and it's very expensive to build a friendly EEG measuring environment. This study attempts to modify a commercial treadmill to be the ground reaction force and EEG measuring device. We applied a band-limited adaptive filter to reduce the gait-related artifacts, performed independent component analysis to eliminate ECG, EOG and EMG artifacts. Next, we used statistical artifacts features to qualify the epoch's quality, such as extreme value, kurtosis and spectral power outliers.

With adaptive filtering, it's significantly reduced EEG spectral power in 1.5 to 8.5Hz frequency range and gait-related harmonics during walking ($p\text{-value}<0.05$). We compared the differences of EEG rhythms between forward and backward walking by hypothesis testing. After forward walking, *Alpha* activity was significantly decreased in F3, P3, P4, O1, O2; and after backward walking, *Alpha* activity significantly decrease in F4, C3, C4, P3, P4. During backward walking, the α_2 and σ activity were significantly lower than forward walking in C3 and C4.

These results demonstrated the different EEG features between forward and backward walking and this measuring platform has the potential to develop more physiological features for rehabilitation.

Keywords: force treadmill, EEG, ICA, gait-related artifact, adaptive filter

Contents

論文審定書	i
致謝	ii
摘要	iii
Abstract	iv
Contents	v
List of Figures	ix
List of Tables	xi
Chapter 1 Introduction	1
1.1 Background	1
1.2 Motivation	1
1.3 Organization of This Thesis	3
Chapter 2 EEG and Artifacts	4
2.1 Brain and Electroencephalogram	4
2.1.1 EEG Rhythms	5
2.1.1 EEG Asymmetry	6
2.2 Signal Artifacts	7
2.2.1 Intrinsic Artifacts	7
2.2.2 Gait-related Artifacts	8
Chapter 3 Experiment Equipment and Methods	10
3.1 Force Treadmill	10
3.1.1 Treadmill Architecture	10

3.1.2 Treadmill Modeling.....	11
3.1.3 Ground Reaction Force Estimation	11
3.2 ECG Measuring Device and Method	12
3.3 EEG Measuring Device and Method	13
3.4 Experiment Flow.....	13
 Chapter 4 EEG Artifacts Removal	15
4.1 Signal Preprocessing	16
4.1.1 Synchronization.....	17
4.2 Gait-Related Artifacts Removal.....	19
4.2.1 LMS Adaptive Filters	19
4.2.2 Band Limited LMS Adaptive Filter.....	20
4.3 Visual Inspection	21
4.4 Independent Component Analysis	22
4.4.1 Blind Source Separation	22
4.4.2 Entropy and Mutual Information.....	23
4.4.3 Information Maximization ICA (Infomax ICA)	25
4.4.4 Removing ICA Components.....	26
4.5 Statistical Artifacts Removal.....	28
4.5.1 Epochs.....	28
4.5.2 Time-Domain Statistical Analysis	30
4.5.3 Frequency-Domain Statistical Analysis	32
 Chapter 5 EEG Spectrum Analysis	33
5.1 EEG Power Spectrum Density Estimation	33
5.2 EEG Rhythms Analysis	34

5.2.1 EEG Rhythms	34
5.2.2 EEG Rhythm Increment.....	35
5.2.2 EEG Rhythm Asymmetry.....	35
5.3 Statistical Hypothesis Test	35
5.2.1 Hypothesis Tests for Dependent Samples.....	37
Chapter 6 Experimental Results.....	38
6.1 Performance of Gait-related Artifact Removal	38
6.1.1 Spectral Power Ratio	38
6.1.2 Mode Power Ratio.....	38
6.1.3 Results.....	40
6.2 EEG Rhythm Analysis	42
6.2.1 Forward Walking.....	42
6.2.2 Backward Walking	43
6.2.3 Forward Walking versus Backward Walking.....	44
6.3 EEG Asymmetry Analysis	47
6.3.1 Forward Walking.....	47
6.3.2 Backward Walking	48
6.3.3 Forward Walking versus Backward Walking.....	48
Chapter 7 Discussion and Future Works.....	50
7.1 Performance of Gait-related Artifacts Removal	50
7.2 Different EEG Patterns in Forward and Backward Walking	51
Reference	54
Appendix.....	60
Appendix I Gait-related Artifacts.....	60

Appendix II EEG Rhythms (Relative Power).....	66
Appendix III EEG Asymmetry (Relative Power)	74
Appendix IV EEG Amplitude Spectrum (Absolute Power)	76

List of Figures

Figure 2-1 10-20 system and brain lobes	5
Figure 3-1 Force treadmill and force plate	10
Figure 3-2 GRF measuring circuit	10
Figure 3-3 Concept of treadmill modelling	11
Figure 3-4 Ground reaction force estimation.....	11
Figure 3-5 ECG measuring circuit architecture	12
Figure 3-6 ECG measurment	13
Figure 3-7 Experiment illustration.....	14
Figure 3-8 Experiment flow.....	14
Figure 4-1 Artifacts removal flow.....	15
Figure 4-2 Signal preprocessing flow	16
Figure 4-3 Pacing mark.....	17
Figure 4-4 Pacing artifacts detection in EEG signals	18
Figure 4-5 Correlation coefficient.....	18
Figure 4-6 Typical adaptive filter structure.....	19
Figure 4-7 Modified adaptive filter structure.....	21
Figure 4-8 Abnormal interval in EEG signals.....	21
Figure 4-9 Reject boundary	22
Figure 4-10 Cocktail party problem.....	22

Figure 4-11 The situation of non-invasive EEG measurement	23
Figure 4-12 Mutual information and entropy	24
Figure 4-13 Single layer neural network	25
Figure 4-14 Independent components.....	27
Figure 4-15 (a) Removed ICA components	27
Figure 4-15 (b) Removed ICA components	28
Figure 4-16 Epoch segmentation in standing condition	29
Figure 4-17 Epoch segmentation in walking condition	29
Figure 4-18 Statistical artifacts removal process flow.....	30
Figure 4-19 PDF shape of super-Gaussian, Gaussian and sub-Gaussian	31
Figure 5-1 Three periods in the experiment.....	33
Figure 5-2 EEG rhythms and frequency bands	34
Figure 5-3 Two-tail hypothesis test.....	36
Figure 6-1 GRF signal and spectrum	39
Figure 6-2 Ensemble channel-average PSD (Subject H)	40
Figure 6-3 Ensemble channel-average NPSD (Subject H)	41
Figure 6-4 The power ratios of EEG data	41

List of Tables

Table 2-1 Brain lobes and functions	4
Table 2-2 EEG rhythms and frequency bands	5
Table 5-1 Type I error and Type II error	36
Table 6-1 Dependent <i>t</i> -Test results of power ratios	41
Table 6-2 EEG activities of forward walking (comparing after to before periods).....	43
Table 6-3 EEG activities of forward walking (comparing during to before periods).....	43
Table 6-4 EEG activities of backward walking (comparing after to before periods).....	44
Table 6-5 EEG activities of backward walking (comparing during to before periods)	44
Table 6-6 EEG activities of the before walking periods (comparing backward to forward)	45
Table 6-7 EEG activities of the after walking peridos (comparing backward to forward)	45
Table 6-8 EEG increment after walking (comparing backward to forward).....	46
Table 6-9 EEG activities during walking (comparing backward to forward)	46
Table 6-10 EEG increment during walking (comparing backward to forward).....	47
Table 6-11 EEG asymmetry on forward walking (after versus before walking)	47
Table 6-12 EEG asymmetry on forward walking (during versus before walking)	47
Table 6-13 EEG asymmetry on backward walking (comparing after to before).....	48
Table 6-14 EEG asymmetry on backward walking (comparing during to before).....	48
Table 6-15 EEG asymmetry before walking (comparing backward to forward)	49

Table 6-16 EEG asymmetry after walking (comparing backward to forward)	49
Table 6-17 EEG asymmetry during walking (comparing backward to forward)	49
Table 7-1 GRF bandwidth (unit: Hz)	50
Table 7-2 GRF f_0 (unit: Hz)	50
Table 7-3 Median heart rate during walking (unit: bpm)	52

Chapter 1

Introduction

1.1 Background

According to World Health Organization (WHO), stroke (cerebrovascular accident) is the third leading causes of years of life lost (YLL) in the world in 2012. In addition, according to Taiwan Ministry of Health and Welfare, stroke rank number 3 in top ten causes of death in 2013. Furthermore, stroke is also the third causes of death (8.4%) in the elderly population aged over 60. Since Taiwan's population is aging gradually, the rehabilitation of stroke patients is an important issue nowadays.

The obstruction of the blood flow to the brain is the cause of stroke and often results in brain malfunctioning. The symptoms of the stroke include memory loss, muscle weakness and perception deterioration, etc. Lots of these symptoms can lead to movement inability or motor coordination disorder that may result in inconvenient life to patients.

Moreover, about 50% to 70% stroke patients have tumble experiences. The stroke patients have high tumbling risk due to the poor balancing ability. Hence recovering the walking ability is an important training goal for rehabilitation.

1.2 Motivation

Locomotion is a complicated dynamic interaction between motor planning and feedback. In recent years, treadmill walking has been chosen as a gait rehabilitation method. Recent studies showed that treadmill backward walking can improve stroke patient's balance ability, gait performance and cardiopulmonary fitness [1].

There are differences between forward and backward walking. For example, the

gait-cycle sequence and knee movement direction of backward walking were reversed to forward walking [2-3]. Researchers showed that backward walking possesses some advantages relative to forward walking, such as improve balance ability [4], increase muscle activities [5], strengthen knee extensor [6] and reduce patellofemoral joint compressive forces [7].

Previous studies showed that the control of locomotion is related to cortical activities [8]. Electroencephalograph (EEG) is a valuable tool for studying and diagnosing the cortical activities. EEG measures voltage fluctuations resulting from the brain activities. However, the voltage fluctuation of EEG is about 5 to $30\mu\text{V}$ and thus can be easily contaminated by 50/60Hz noise, eyes blinking, electrooculography (EOG), and electrocardiography (ECG or EKG), etc. Moreover, during walking, EEG will be affected by electromyography (EMG) and gait-related artifacts.

For the sake of estimating gait-related artifacts during walking, force measuring treadmills have been introduced to measure the ground reaction force. Although there are many force treadmills at present, these treadmills were designed to be rigid and heavy in order to increase treadmill's natural frequency. These custom-made treadmills are not popular due to the high manufacturing cost. This is also the reason why it is very expensive to build a friendly EEG measuring environment under locomotion.

Considering the convenience and cost of conventional force treadmills, this thesis attempts to modify a commercial treadmill into a ground reaction force and EEG measuring device. This work also tries to improve the fidelity of the measured EEG signal. The final goal is to analyze the differences between the EEG signals of forward and backward walking.

1.3 Organization of This Thesis

In Chapter 2, the relationship between EEG and brain function will be briefly described. The EEG artifacts and the corresponding artifact removal techniques will also be introduced in this chapter.

Chapter 3, the modeling method for the force treadmill and the EEG, ECG measuring device will be described. In addition, the architecture of the EEG measuring and processing system will also be presented in this chapter.

Chapter 4, introduces the EEG artifact-removal and processing method. In specific, the filtering algorithms, including band-limited LMS adaptive filter and Infomax ICA method will be briefly introduced.

In chapter 5, we will briefly describe the measures of EEG rhythm, such as α , β , etc. Furthermore, EEG spectrum and EEG rhythms estimation methods will also be explained in this chapter.

The results of the experiments will be shown in chapter 6 and discussions will be presented in chapter 7.

Chapter 2

EEG and Artifacts

Many functional neuroimaging studies have shown that the cortical activities play an important role in leg movement and locomotion [9-12]. These imaging method, including functional magnetic resonance imaging (fMRI) and functional near-infrared spectroscopy (fNIRS), provide a good spatial but poor temporal resolution. In contrast, Electroencephalogram (EEG) can study the dynamics of the brain with a very good time resolution. However, EEG signals are noisy and difficult to measure by non-invasive method. The following sections will briefly introduce the artifacts and the physiological meaning of the EEG signals.

2.1 Brain and Electroencephalogram

Brain could be divided into four major lobes, each of which corresponds to different brain locations and functions. Increasing EEG activity could be observed when the brain is processing certain actions. A concise summary is given in Table 2-1.

Table 2-1. Brain lobes and functions

Lobe	Actions
Frontal lobe	Conscious thought, emotion, motor planning
Parietal lobe	Motor control, spatial information processing
Occipital lobe	Visual processing
Temporal lobe	Language recognition, audio and olfactory processing

Brain activity can be recorded by non-invasive EEG measuring method. This work studies places the scalp electrodes on the location specified by the international 10-20 system (Figure 2-1). The system is based on the relationship between the

location of the electrode and the underlying region of the cortex.

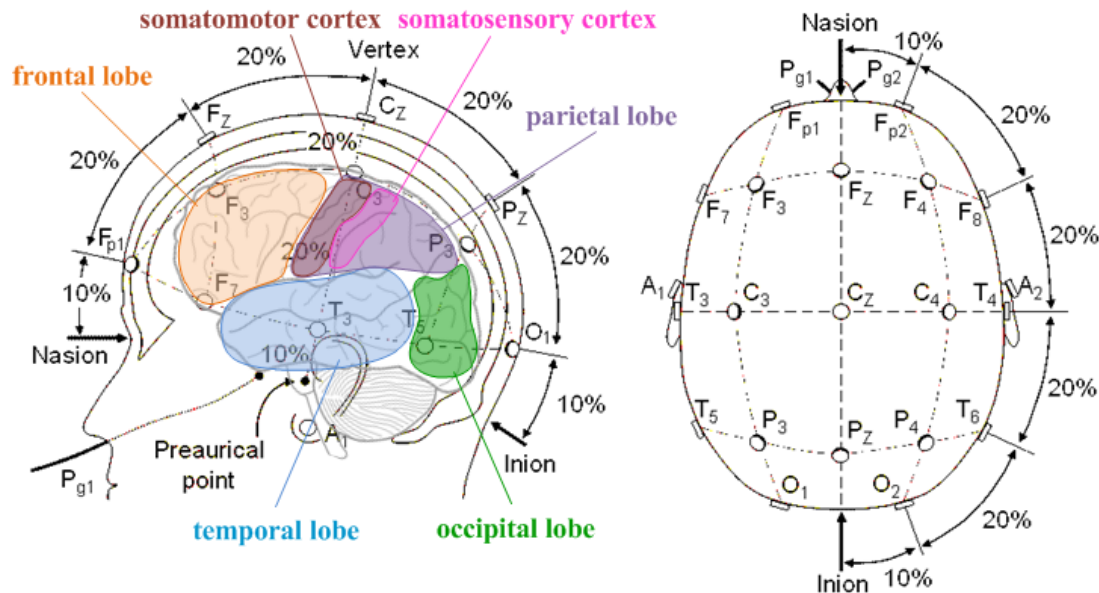


Figure 2-1. 10-20 system and brain lobes

2.1.1 EEG Rhythms

The spectrum of the recorded EEG can be decomposed into different frequency bands results in different EEG rhythms. Table 2-1 shows typical EEG rhythms and the corresponding frequency bands:

Table 2-2. EEG rhythms and frequency bands

Rhythms	<i>Delta</i>	<i>Theta</i>	<i>Alpha</i>	<i>Beta</i>	<i>Gamma</i>
Frequency band	1-4 Hz	4-8 Hz	8-12Hz	12-30Hz	40-50Hz

We can observe the changes of rhythmic activities to infer the cortical activities. The decrease of EEG rhythmic power is considered to be a decrease in synchrony of the underlying neuronal populations, which is called event-related desynchronization (ERD). In contrast, the increase of EEG rhythmic power suggests a large populations of neurons oscillate in synchrony, which is called event-related synchronization (ERS). For example, *Alpha* ERS reflects a brain in state of reduced information processing or

‘idling’, which could be found in occipital region when eyes closed.

The effects of locomotion on alpha and beta rhythm power have been investigated in a numbers of previous studies. Researchers showed that ERD corresponds to motor planning and movement executing. The alpha (8-12Hz) and beta (18-26Hz) ERD were strongest above the central region during forward walking [13]; the alpha (8-12Hz) and beta (12-25Hz) ERD were also observed near the motor cortex during backward walking (around electrode C4) [14-15]. Moreover, the decrease of beta power relative to the baseline level (i.e., resting condition) is considered a reliable indicator of the movement execution and motor imaginary [16].

It has also been shown that the exercise intensity and mode could affect EEG rhythmic activity [17]. In moderate intensity exercise, an increase of alpha activity in parietal region appeared after “familiar exercise” and “unfamiliar exercise” modes, but a significant increase of beta activity in the parietal cortex was found only after the “unfamiliar exercise” mode.

This study hypothesizes that the ERD of backward walking are stronger than forward walking. In addition, an increase of beta rhythm in parietal region will be found after backward walking as it is an “unfamiliar exercise” mode.

2.1.2 EEG Asymmetry

An EEG asymmetry index was derived for both frontal and parietal regions. The spectral power difference between right and left hemispheres is used to calculate the asymmetric scores. Higher asymmetry scores represent greater activity in left hemisphere.

There are two models for EEG asymmetry: valence model and direction model. In valence model [18], the activation of right frontal region reflects the negative valence, such as fear and anger. In contrast, the left frontal region reflects the

positively valence, such as pleasure and joy. In direction model, the right frontal region is associated with avoidance motivations and left frontal region is associated with approach motivations. Apparently, there is a contradiction between two models: anger is not only a negative valence emotion but also an approach motivation [19].

The suitable model for the EEG asymmetry is still not concluded. However, at current time, the results of many exercise studies supports direction model. Previous studies showed that greater relative left frontal activity predicting lower energetic arousal, and the low energetic arousal could be a predictor of approach motivation [20-21]. It was also demonstrated that great relative left frontal activity predicted tiredness and calmness during recovery from exercise, and this ‘calm-tiredness’ is possibly an approach emotion [22]. Another research reported that the right frontal alpha1 (7.5-10Hz) activity were significantly higher after exercise than before, and it might be associated with approach emotion [23].

We expected that the backward walking mode would result in higher left frontal activity due to the higher exercise intensity than forward walking.

2.2 Signal Artifacts

2.2.1 Intrinsic Artifacts

The signal artifacts refers to unwanted signals mixing with the desired signal. There are usually three intrinsic artifacts appearing in EEG signals:

- 1) ECG artifacts: Electrocardiogram (ECG) can easily affect the EEG due to the relatively high electrical field. The interference on the EEG could be observed by the periodicity and coincidence with the ECG R-peaks.
- 2) Eyes blinking artifacts: The eyes blinking are hardly avoided in ‘eyes open’ condition. When the eyes are blinking, the electric field around the eyes will propagate over the scalp, and its projection on the scalp follows the

anterior-posterior direction.

- 3) Muscle artifacts: The neck or facial electromyography (EMG) are the main muscle artifact sources on EEG. The frequency band of EMG overlaps with EEG (from 0 to >200Hz) [24], so it could not be corrected by frequency filtering without EEG information loss.

Fortunately, the above artifact sources are spatially stationary, which could be removed from EEG by ICA method effectively [25].

2.2.2 Gait-related Artifacts

The motion artifacts are produced by the movement of body. In ambulatory condition, gait-related artifacts can corrupt the EEG signals. The motion harmonics can be clearly observed in EEG spectrum, and the fundamental frequency of the harmonics is consistent with the step frequency [26]. Unfortunately, these motion artifacts are not limited to a narrow frequency band and can't thus be removed by a simple frequency filter.

There are several gait-related artifacts removal approaches which can be divided into three categories: template subtraction [27], ICA decomposition [28] and adaptive filtering [29].

Template subtraction method uses an ‘ideal template’ to estimate the artifact in each epoch. The EEG signals were segmented in stride cycles at first. For each epoch, the ‘ideal template’ was computed by averaging the neighboring 20 time-warped epochs. The template is apparently not the exact artifacts that contaminate the signals, and can therefore introduce additional noise into the epoch [30].

ICA is a powerful tool for artifacts removal. However, unlike most spatially stationary artifacts, gait-related artifacts can't be removed by a small subsets of ICA components. Its application requires high-density EEG records and it also requires a lot

of memory and computational time.

By using adaptive filter as a noise canceller, previous approaches has placed accelerometer was placed on the electrode cap in order to record the movement of the head. Consequently, gait-related artifacts can be estimated from these kinematic data. Instead of wearing additional sensors, this study modified a commercial treadmill to record the ground reaction force (GRF) in order to estimate the gait-related artifacts.

Chapter 3

Experiment Equipment and Method

3.1 Force Treadmill

3.1.1 Treadmill Architecture and Data Acquisition

As shown in Figure 3-1, the commercial treadmill was equipped with four load cells at four support legs. The measured GRF was calculated by summing the load cell signals. For treadmill modelling, a force plate was placed above the belt in order to measure the input signals of the treadmill.

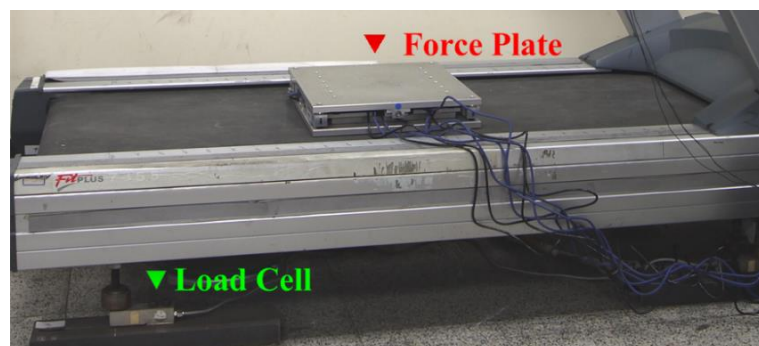


Figure 3-1 Force treadmill and force plate

A four-channel measuring circuit was constructed. By using OP-177, the load cell signals were amplified 1000 times by the circuit shown in Figure 3-2. Data were recorded by National Instrument (NI) NI-9234 with a sampling frequency of 512Hz.



Figure 3-2 GRF measuring circuit

3.1.2 Treadmill Modeling

The frequency domain identification method has been employed for treadmill modelling [31]. The concept was briefly introduced in Figure 3-2:

1. Excite the force plate to generate a quasi-impulse response of the treadmill.
2. Apply the fast Fourier transform (FFT) to the input signal $x(t)$ and output signal $y(t)$ to obtain the spectra of the input and output signals.
3. Divide $Y(\omega)$ by $X(\omega)$ to obtain treadmill model $G(\omega)$.

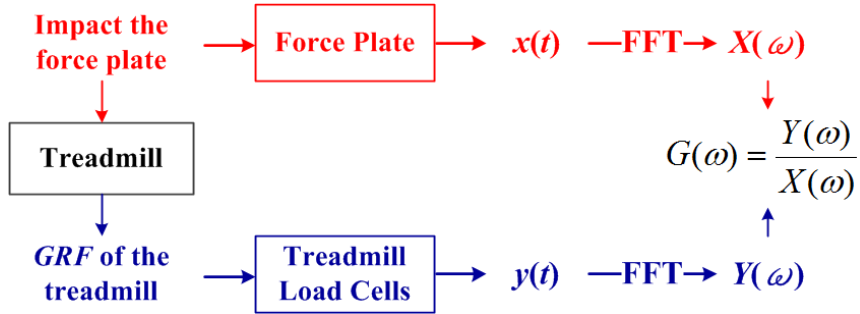


Figure 3-3 Concept of treadmill modelling

3.1.3 Ground Reaction Force Estimation

The concept of ground reaction force estimation was illustrated in Figure 3-4:

1. Apply FFT to the treadmill output signal $y(t)$ to obtain $Y(\omega)$.
2. Divide $Y(\omega)$ by $G(\omega)$, then perform inverse fast Fourier transform (IFFT) and apply a 4th order Butterworth low-pass filter to the estimated GRF $x_s(t)$.

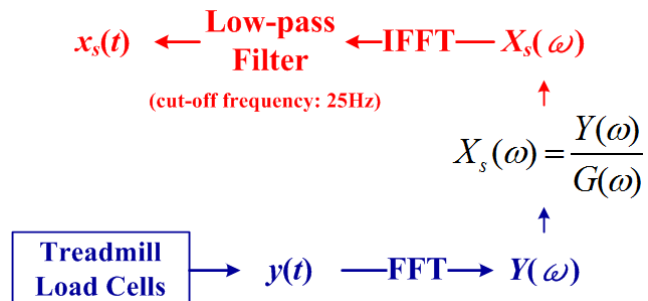


Figure 3-4 Ground reaction force estimation

The cut-off frequency of the low-pass filter was set to 25Hz since the bandwidth of the walking ground reaction force is lower than 25Hz.

3.2 ECG Measuring Device and Method

The ECG measuring circuit architecture was showed in Figure 3-5. The right leg drive loop was used to eliminate the common-mode interference. The inputs from differential mode channels pass into an Analog Device AD620 instrumentation amplifier, then the resulting signal is passed into the frequency filter; the cutoff frequency of the high-pass filter is 0.05Hz and the low-pass filter is 100Hz.

The common-mode electrode was placed on the right arm, negative electrode placed on the left chest (precordial leads V5), and positive electrode was placed on the right shoulder, as shown in Figure 3-6. The circuit output signal was recorded by NI-9234 and sampled at 512Hz.

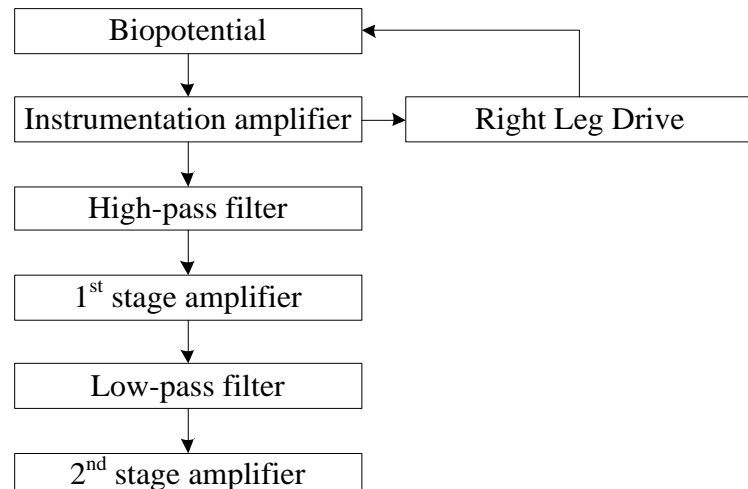


Figure 3-5 ECG measuring circuit architecture

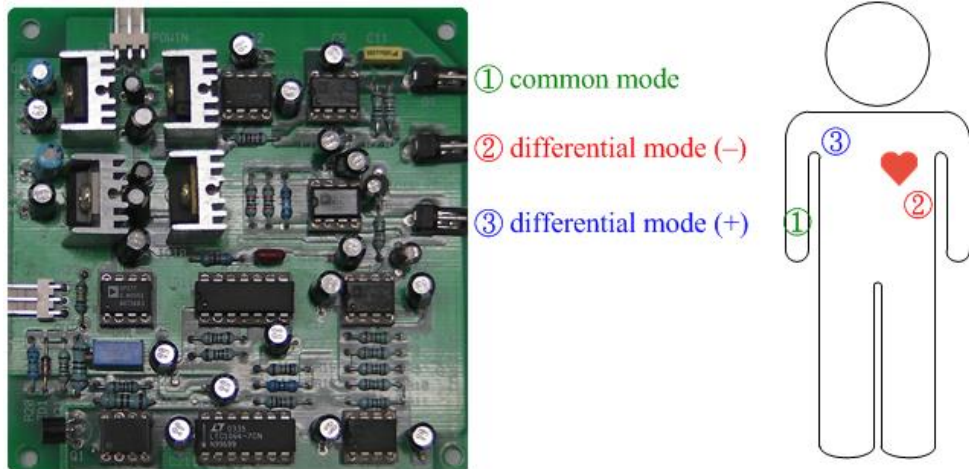


Figure 3-6 ECG measurement

3.3 EEG Measuring Device and Method

Taxes Instrument ADS1299 EEG Front-End Performance Demonstration Kit (TI-ADS1299EEG-FE) was used to record EEG data with a sampling rate of 250Hz. The eight electrodes were attached at F3, F4, C3, C4, P3, P4, O1 and O2 specified by international 10-20 system. The reference electrode was placed on Cz.

3.4 Experiment Flow

The experimental environment was setup as Figure 3-7. Two tennis balls were hung to the ceiling which are the space references for the subjects. For the sake of reducing the motion artifacts, the EEG cables were secured in a flexible tube and the measuring device was packaged and fastened on the subject's waist. The EEG, ECG and GRF signals were recorded simultaneously.

Nineteen graduate students (eighteen males and one female, age range 22-31 years) were instructed to do the following tasks during experiment:

1. Chewing and blinking as little as possible.
2. Standing on the treadmill in a relax position and keeping the eyes on the tennis ball.
3. Try to maintain the same distance between the body and tennis ball during

walking.

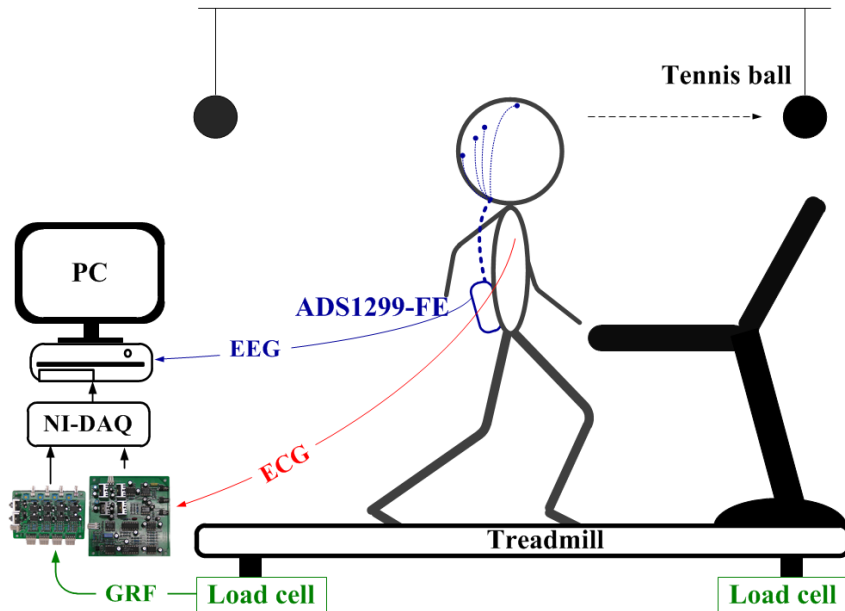


Figure 3-7. Experiment illustration

Two walking tasks were performed by the participants: forward walking and backward walking. In forward walking, subjects stood on the treadmill and faced the front of the treadmill in the first 3 minutes, walked at a speed of 3km/h in the next 4 minutes and then stood on the treadmill in the final 3 minutes. In backward walking, subjects had to turn around with its back facing the front end of the treadmill. The sequence of the backward walking task is identical with the forward walking. The experimental procedure was graphically shown in Figure 3-8:

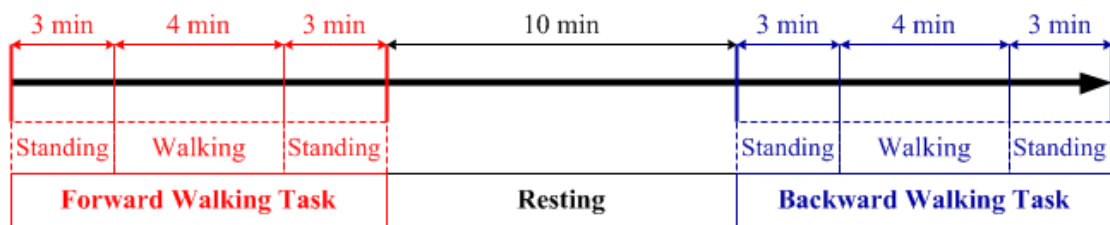


Figure 3-8 Experiment flow

Chapter 4

EEG Artifacts Removal

The measured signals were processed by the procedure shown in Figure 4-1 and performed by MATLAB (MathWorks Inc.). The signal preprocessing is a preparing step for the adaptive filtering, independent component analysis (ICA) and statistical artifacts removal processes. LMS adaptive filtering was only performed in walking EEG signals, the purpose of this step is to reduce the gait-related artifacts.

The abnormal interval in EEG data were first removed by visual inspection. Next, ICA was applied to separate the artifacts and EEG signal. Lastly, we performed statistical artifact removal in order to remove the abnormal epochs which are statistically very different from the remaining epochs. The details will be explained and illustrated in the following sections.

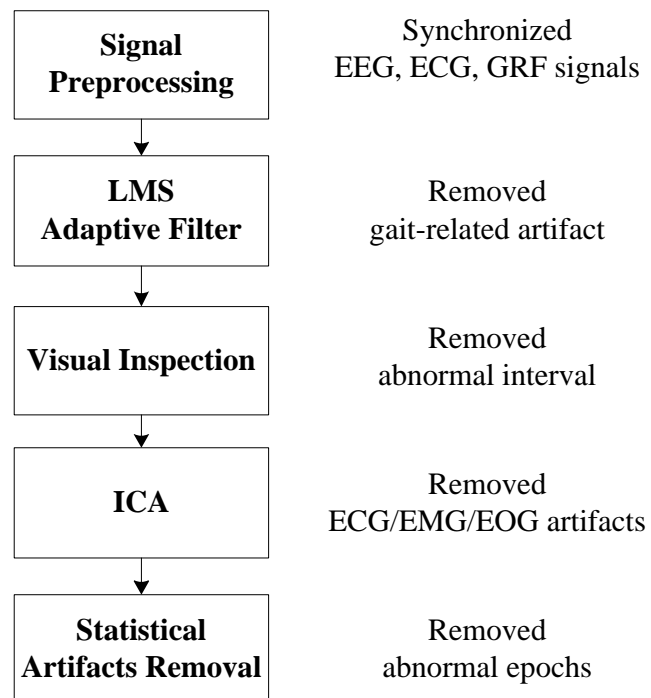


Figure 4-1 Artifacts removal flow

4.1 Signal Preprocessing

As shown in Figure 4-2, EEG signals were sampled at 250Hz, low-pass filtered at 50Hz, high-pass filtered above 0.9Hz and notch filtered at 60Hz.

ECG signals were then resampled from 512 Hz to 250Hz in order to synchronize with EEG sampling rate. The sampling rate conversion rational factor $I / D = 250/512 = 125/256$. The resampling procedure will first perform the interpolation by the factor $I=125$, followed by a FIR (finite impulse response) filter and then decimated the output of the filter by the factor $D = 256$ [32]. After the resampling procedure, the signals was processed with medium filter to removal of the baseline wandering which was induced by respiration [33].

GRF signal was estimated by the inverse-dynamic method which was described in Section 3.1.3 and resampled from 512Hz to 250Hz.

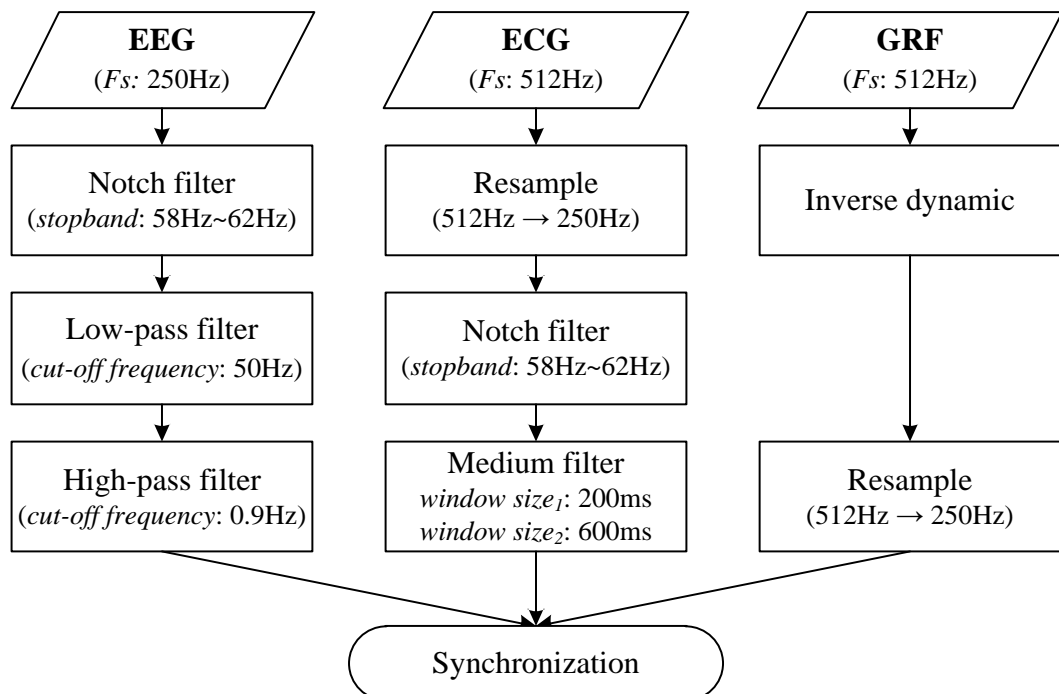


Figure 4-2. Signal preprocessing flow

4.1.1 Synchronization

Because the recording device of EEG (TI-ADS1299EEG-FE) was different from that of GRF and ECG (NI-9234), signal synchronization is needed before performing adaptive filtering and independent component analysis (ICA).

In the experiment, the subjects paced on the treadmill at 5th second in order to generate a ‘pacing mark’, as shown in Figure 4-3. A Common-Average Reference (CAR), which is an ensemble average of the EEG signals was calculated.

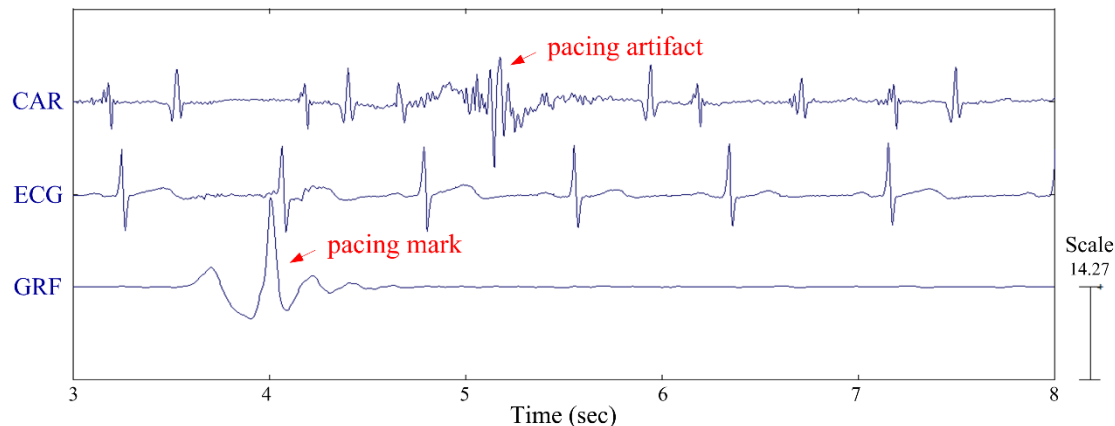


Figure 4-3. Pacing mark

The short-time Fourier transform (STFT) was applied to find the time of pacing in CAR. In applying the STFT, the width of the rectangular window was chosen 0.1 second and was then zero-padding to 1 second. The step size of the moving window was one sample point. As shown in Figure 4-4, the timing of the maximum spectral power is the approximate alignment timing. The difference between the timing of GRF pacing peak and approximate alignment timing is the approximate delay time.

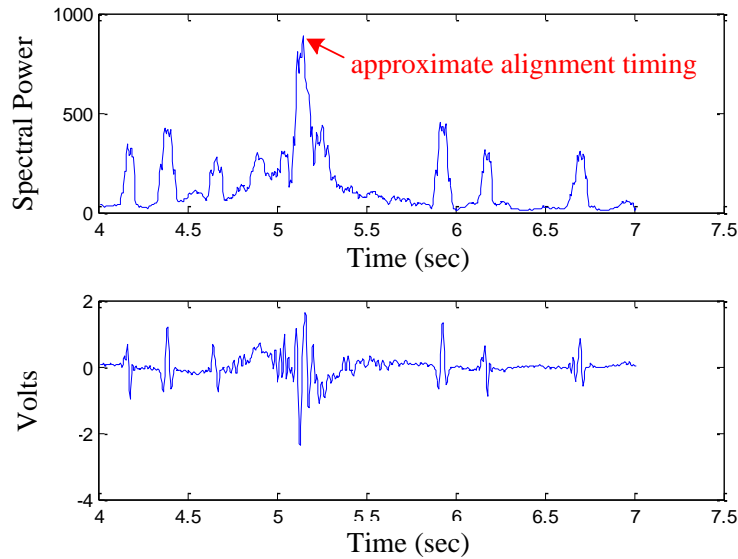


Figure 4-4. Pacing artifacts detection in EEG signals

Next, the correlation between ECG and CAR signal was computed by moving the ECG signal around the approximate alignment timing (0.5 second ahead and after). As shown in Figure 4-5, we chose the timing of maximum correlation coefficient as the fine alignment timing. Then, the summation of the approximate alignment and fine alignment timing is the time delay between the two recording devices.

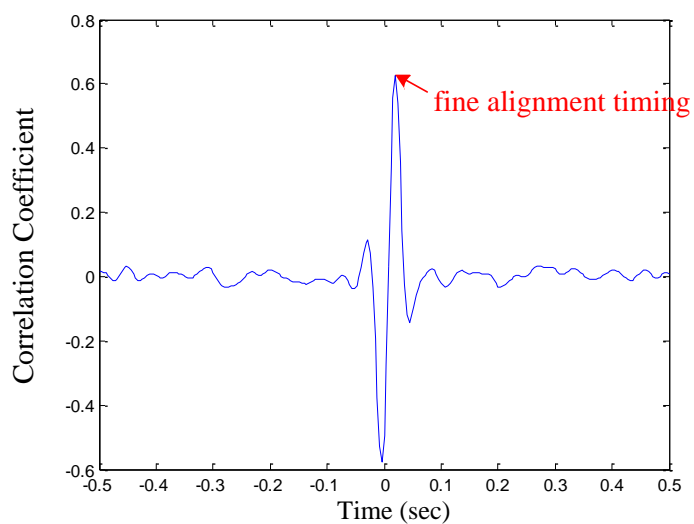


Figure 4-5. Correlation coefficient

4.2 Gait-related Artifacts Removal

4.2.1 LMS Adaptive Filter

Least mean-square (LMS) algorithm was developed by Widrow and Hoff in 1960.

This algorithm is based on the steepest descent method. Due to its robustness and simplicity, it has been widely employed in many applications.

A typical adaptive filter structure is showed in Figure 4-6, the noise source $u(n)$ is fed to an adaptive filter, the adaptive filter tries to simulate the noise path. As a result, the filter output $y(n)$ can approximate the contaminating noise $v(n)$. Consequently, we can use the restored signal $e(n)$ to estimate the signal source $s(n)$.

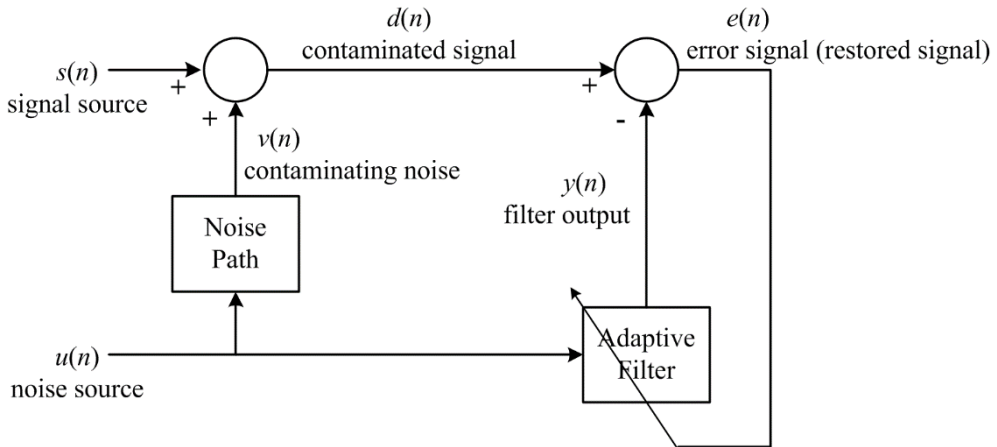


Figure 4-6. Typical adaptive filter structure

We choose an M th order FIR filter structure for the noise path system model.

The output of the filter is given by:

$$y(n) = \hat{w}^T (n-1) u(n) \quad (4.1)$$

where $u(n) = [u(n) \ u(n-1) \cdots u(n-M+1)]^T$ is a vector of input signal samples,

$w(n) = [w_0 \ w_1 \cdots w_{M-1}]^T$ is a vector containing coefficients of the FIR filter at time n .

The purpose is to find the suitable weight vector $w(n)$ that can represent the unknown noise path system. The update rule (tape-weight adaptation) of the weight vector is:

$$w(n+1) = \hat{w}^T(n) + \mu [u(n)e(n)] \quad (4.2)$$

$$e(n) = d(n) - \hat{w}^T(n)u(n) \quad (4.3)$$

where μ is the learning rate of the adaptive filter, and we determine μ by [34]:

$$\begin{aligned} \mu &= \frac{\mu_0}{M\sigma_u^2} \\ \sigma_u^2 &= \text{variance of filter input vector} \\ \mu_0 &= 0.1 \sim 0.01 \end{aligned} \quad (4.4)$$

In this way, the adaptive filter will continuously update the weight vector and minimize the estimation error $e(n)$ in order to choose the optimal weight for the filter.

4.2.2 Band Limited LMS Adaptive Filter

In the case of gait-related artifact removal, the ground reaction force can be viewed as the noise source $u(n)$ and measured EEG is the contaminated signal $d(n)$ in Figure 4-6.

GRF is a narrowband signal whose bandwidth is about 8.5Hz. However, the sampling frequency of the measured EEG is much higher than 8.5Hz.

For the sake of reducing the order of adaptive filter, the structure of adaptive filter is modified as Figure 4-7. The cut-off frequency of low-pass filter is set to 8.5Hz because it encompassed the step frequency and its first two harmonics [27]. Next, both $u(n)$ and $d_L(n)$ are resampled from 250Hz to 50Hz to avoid quantization error. The resample method was the same as Section 4.1.

The up-sampled $y_d(n)$ represents estimated gait-related artifact $y_u(n)$. Subtracting $y_u(n)$ from $d(n)$ yields the restored signal $r(n)$. In this study, we chose 3rd order adaptive filter for backward walking and 9th order for forward walking to simulate the noise path.

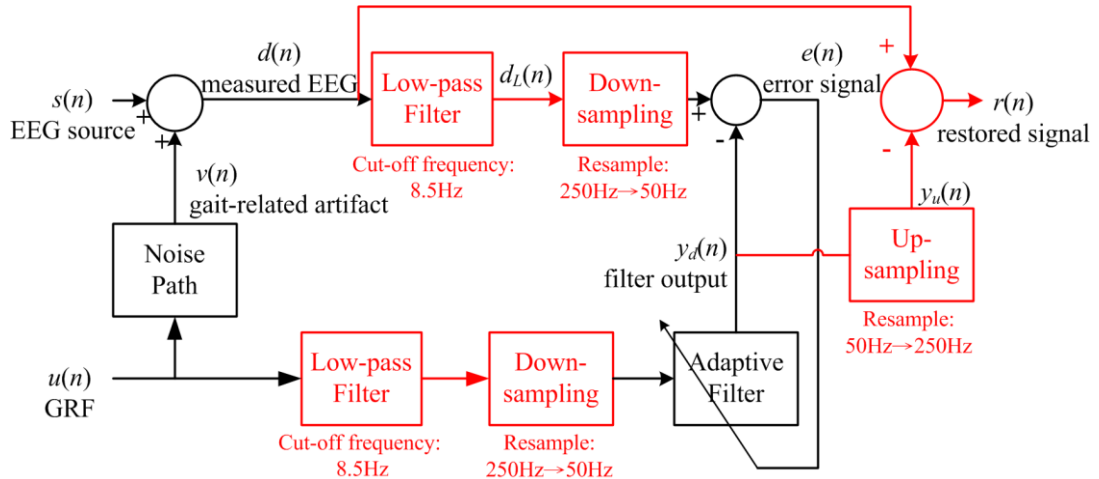


Figure 4-7. Modified adaptive filter structure

4.3 Visual Inspection

There are some unpredictable artifacts in EEG data. These artifacts may be treated as independent components by ICA. To remove these artifacts, visual inspection was performed before independent component analysis in order to eliminate the interferences on the weight matrix adjustment of ICA. For example, in Figure 4-8, the highlighted data regions were treated as the abnormal interval because the trend at P3 channel is different from the other channels. After removing the interval, a reject boundary was marked to indicate signal discontinuities. This procedure was performed in the EEGLAB toolbox scroll viewer [35], as shown in Figure 4-9.

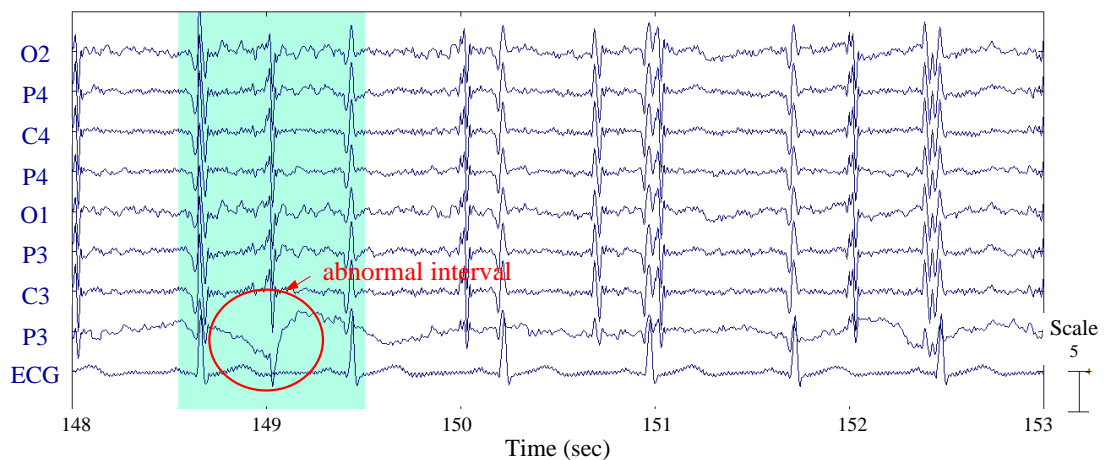


Figure 4-8. Abnormal interval in EEG signals

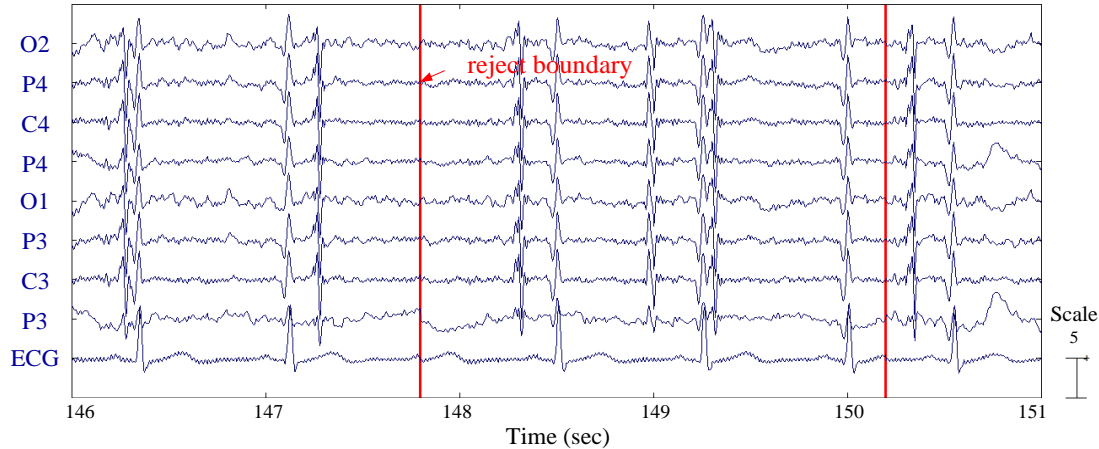


Figure 4-9. Reject boundary

4.4 Independent Component Analysis

Independent Component Analysis (ICA) is a well-known method of blind source separation (BSS), which is used to separate the unknown mixed signals.

4.4.1 Blind Source Separation

One of the famous models of BSS is the cocktail party problem where a crowded room with many people speaking at the same time and the listener (receptor) is trying to follow one of the voice source, as illustrated in Figure 4-10.

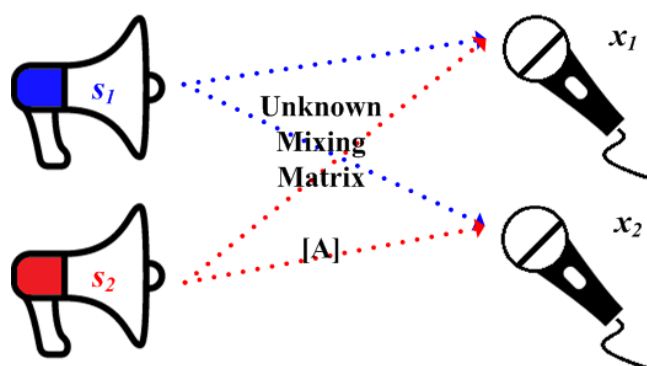


Figure 4-10. Cocktail party problem

Suppose there are two unknown speaking sources s_1 and s_2 , two receptors (microphones) x_1 and x_2 . The relationship of these signals can be expressed as:

$$\begin{aligned}x_1(t) &= a_{11}s_1(t) + a_{12}s_2(t) \\x_2(t) &= a_{21}s_1(t) + a_{22}s_2(t)\end{aligned}\quad (4.5)$$

Eq. (4.5) can be represented in matrix form as:

$$\mathbf{X} = \mathbf{AS} \quad (4.6)$$

Then, S can be obtained via Eq. (4.6) by:

$$\mathbf{S} = \mathbf{A}^{-1}\mathbf{X} = \mathbf{WX} \quad (4.7)$$

We do not know the mixing condition of the measured signals since A is unknown. So we need to solve the demixing matrix \mathbf{W} (inverse matrix of A) to separate these mixed signals.

The problem of EEG measurement is similar to the cocktail party problem. The electrodes are placed on the scalp rather than the brain, so the signals recorded on the scalp are mixtures of the cerebral, as shown in Figure 4-11. In addition, the artifact sources, such as eyes blinking, cardiac signals and muscle noises, are summed linearly to the electrodes. Since these signal sources are statistically independent, we can remove these noises by ICA method.

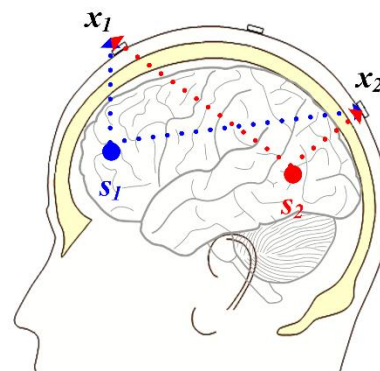


Fig 4-11. The situation of non-invasive EEG measurement

4.4.2 Entropy and Mutual Information

Entropy H is a randomness measure for signals. Suppose random variable x have N observations whose probabilities are p_1, \dots, p_N , respectively [36], its entropy can be

expressed as:

$$\begin{aligned} H(x) &= -p_1 \log p_1 - \cdots - p_N \log p_N \\ &= -\sum p(x) \log p(x) \\ &= -E[\log p(x)] \end{aligned} \quad (4.8)$$

The joint entropy $H(x, y)$ of two random variables x and y can be defined as:

$$H(x, y) = -\sum p(x, y) \log p(x, y) \quad (4.9)$$

where $p(x, y)$ is the joint probability of x and y .

Consider x and y as sets, the relationship of random variables and entropy is shown in Figure 4-12:

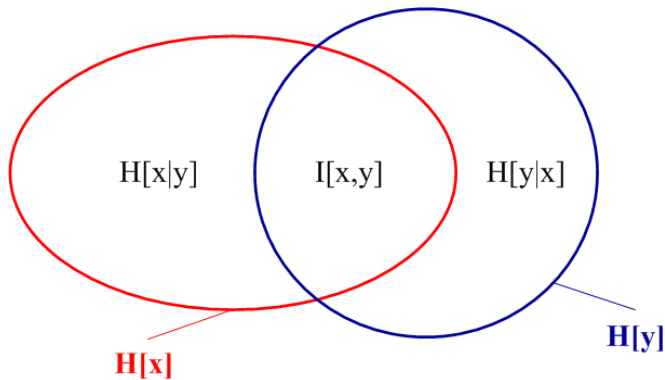


Figure 4-12. Mutual information and entropy

Where $H[x]$ and $H[y]$ are marginal entropies, $H[x/y]$ is the conditional entropy of x given y :

$$H[x | y] = -\sum p(x | y) \log p(x | y) \quad (4.10)$$

So, the mutual information $I(x, y)$ can be expressed as:

$$\begin{aligned} I(x, y) &= H(x) + H(y) - H(x, y) \\ &= H(x) - H(x | y) \\ &= H(y) - H(y | x) \end{aligned} \quad (4.11)$$

When $I(x, y) = 0$, $H(x, y) = H(x) + H(y)$, then x and y are considered to be statistically independent.

4.4.3 Information Maximization ICA (Infomax ICA)

Consider a single layer neural network as shown in Figure 4-13. Infomax ICA separate the mixture by optimizing the matrix \mathbf{W} to maximize the joint entropy of \mathbf{y} .

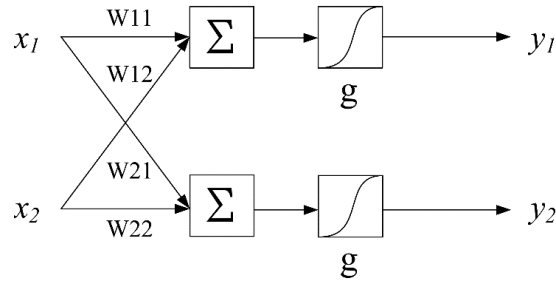


Figure 4-13. Single layer neural network

where

$$\begin{aligned}\mathbf{u} &= \mathbf{Wx} \\ \mathbf{y} &= g(\mathbf{u})\end{aligned}\tag{4.12}$$

In Figure 4-13, the input signals of neural network are the measured signals, the output signals are the estimated sources, \mathbf{W} is the estimated demixing matrix, g is a non-linear function which is a cumulative density function (CDF) of u_i :

$$p(u) = \frac{\partial y}{\partial u}\tag{4.13}$$

The information transmitted by the mapping $f: x \rightarrow y$ can be represented as mutual information between inputs and outputs:

$$I(x, y) = H(y) - H(y | x)\tag{4.14}$$

Differentiating both sides of Eq. (4.14) with respect to \mathbf{W} :

$$\frac{\partial}{\partial \mathbf{W}} I(x, y) = \frac{\partial}{\partial \mathbf{W}} H(y) - \frac{\partial}{\partial \mathbf{W}} H(y | x)\tag{4.15}$$

Since $H(y | x)$ is not affected by \mathbf{W} :

$$\frac{\partial}{\partial \mathbf{W}} H(y | x) = 0\tag{4.16}$$

$$\frac{\partial}{\partial \mathbf{W}} I(x, y) = \frac{\partial}{\partial \mathbf{W}} H(y)\tag{4.17}$$

So, the mutual information $I(x, y)$ can be maximized by maximizing $H(y)$.

The mutual information between the outputs could be expressed as:

$$I(y_1, y_2 \cdots y_n) = \sum_{i=1}^n H(y_i) - H(y) \quad (4.18)$$

When $I(y_1, y_2 \cdots y_n) = 0$, $\sum_{i=1}^n H(y_i) = H(y)$ and $H(y)$ is maximized.

Infomax ICA using gradient method to adjust W in order to maximize $H(y)$:

$$W_{p+1} = W_p + l\Delta W \quad (4.19)$$

where p is the iteration number, l is learning rate, ΔW is the updated weight matrix.

The resulting update rule can be express as:

$$\Delta W = \frac{\partial H(y)}{\partial W} = (W^T)^{-1} + \begin{pmatrix} \frac{\partial p(u)}{\partial u} \\ \frac{\partial u}{p(u)} \end{pmatrix} x^T \quad (4.20)$$

In Eq. (4.20), the computation of inverse matrix is too complicated, so multiplied by $W^T W$ to rescale the update rule:

$$\Delta W = [I - \varphi(u)u^T]W \quad (4.21)$$

$$\text{Where } \varphi(u) = -\begin{pmatrix} \frac{\partial p(u)}{\partial u} \\ \frac{\partial u}{p(u)} \end{pmatrix} x^T.$$

In this study, we used extended-Infomax learning rule for ICA, which could separate sub-Gaussian and super-Gaussian components by the below update rule [37]:

$$\Delta W = \begin{cases} [I - \tanh(u)u^T - uu^T]W & \text{:super - Gaussian} \\ [I + \tanh(u)u^T - uu^T]W & \text{:sub - Gaussian} \end{cases} \quad (4.22)$$

4.4.4 Removing ICA Components

The ICA was performed using the EEGLAB toolbox. The 9-channel physiological signals (8-channels EEG and 1-channel ECG) were decomposed to 9 independent components by extended-Infomax ICA, as shown in Figure 4-14.

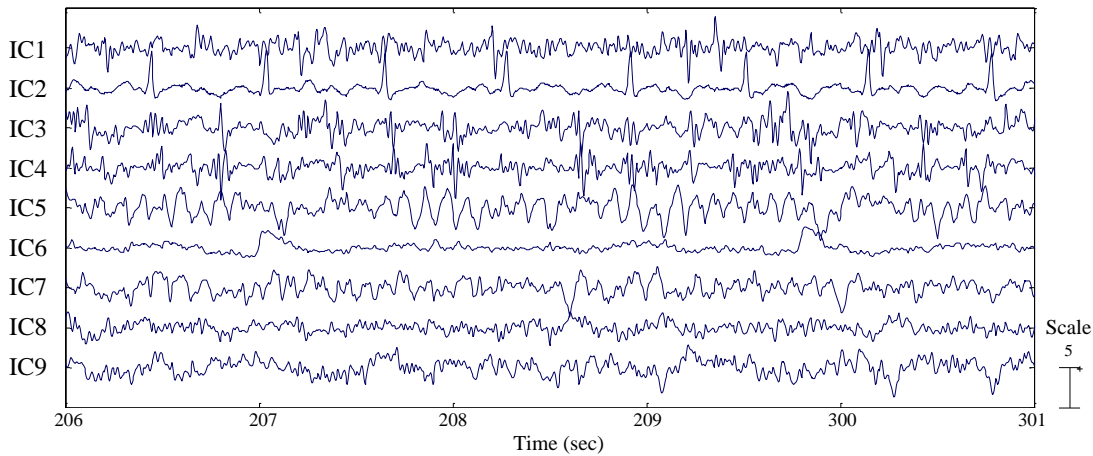


Figure 4-14. Independent components

The scalp map projection of all components will be used here to identify the sources of the components. This procedure was performed with EEGLAB toolbox to remove artificial components by scalp map projection.

As shown in Figure 4-14, background noise (IC1) and ECG artifact (IC2) should be rejected. The noise components usually appear in the leading positions of the component array because they have relatively large amplitude. Eye artifact (IC6) has the smoothly decreasing EEG spectrum and the scalp map shows a strong far-frontal projection. Strong neck muscle EMG (IC3) appears in walking condition, these components show large power at high frequency band (20~50Hz) and showed a stronger projection on O1 or O2 electrodes.

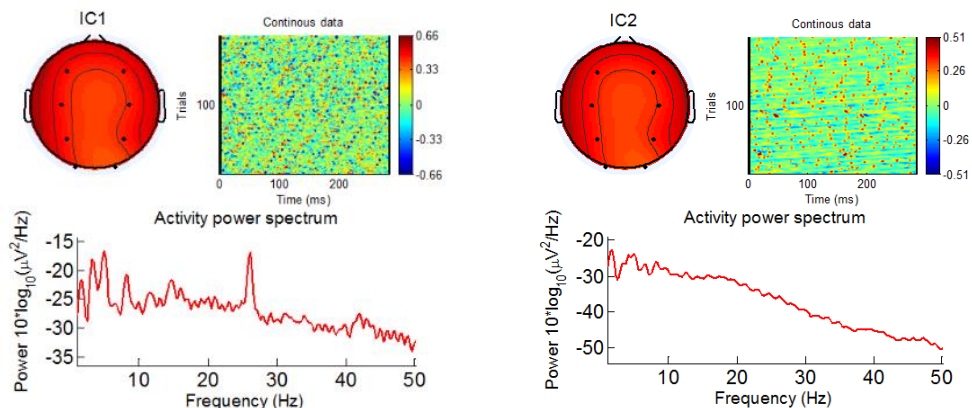


Figure 4-15 (a). Removed ICA components

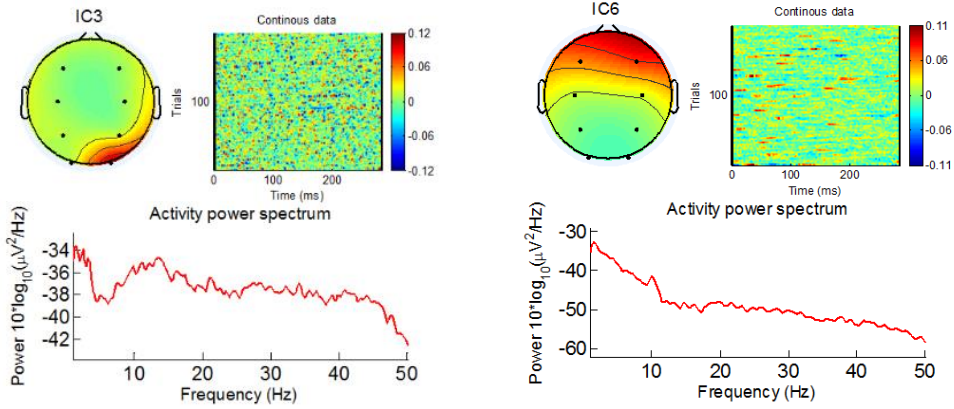


Figure 4-15 (b). Removed ICA components

After removing these artifact components, the new demixing matrix will be applied to reconstruct the EEG signals.

4.5 Statistical Artifacts Removal

4.5.1 Epochs

The time-frequency analysis was employed to help perform the statistical artifacts removal procedure. In standing condition, time-domain EEG signal was truncated by a moving rectangular window (as shown in Figure 4-15):

$$f_w(t) = f(t)w(t) \quad t = 0.5, 1, 1.5, 2 \dots \quad (4.23)$$

$$w(t) = rect(t) = \begin{cases} 1, & t - 0.5 < t < t + 0.5 \\ 0, & \text{else} \end{cases} \quad (4.24)$$

where $f(t)$ is EEG signal, $w(t)$ is the rectangular window function. The windowed data $f_w(t)$ is called epochs. In frequency domain, each epoch was multiplied by a Hamming window, zero-padding (adding dummy samples with a value of 0) to 100 seconds to increase the frequency resolution, and applied fast Fourier transform (FFT) to each one. This procedure is also called short-time Fourier transform (STFT).

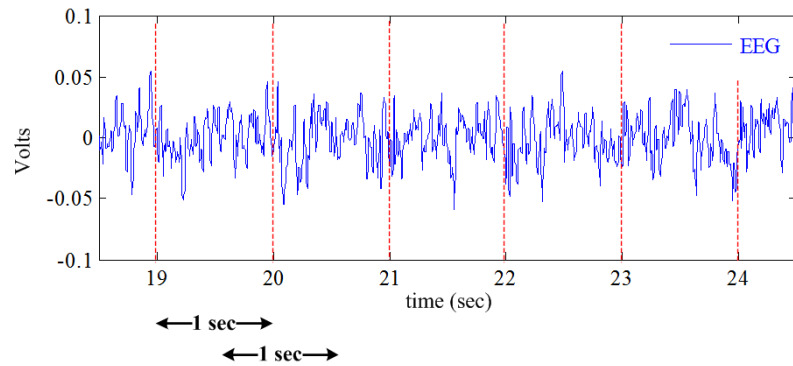


Figure 4-15. Epoch segmentation in standing condition

In walking condition, the EEG signals were divided into epochs of 2 stride cycles and overlapped by 1 stride cycle, as shown in Figure 4-16. The GRF signal was first processed by removing its mean value. The nearest zero-crossing point to heel-strike peak of the GRF signal was selected as the boundary point between the neighboring steps. The interval between the two such boundary points represents a step cycle and two consecutive steps were defined as a stride cycle. These epochs were also multiplied by a Hamming window first, then zero-padding to 100 seconds and applied fast Fourier transform (FFT) to each one.

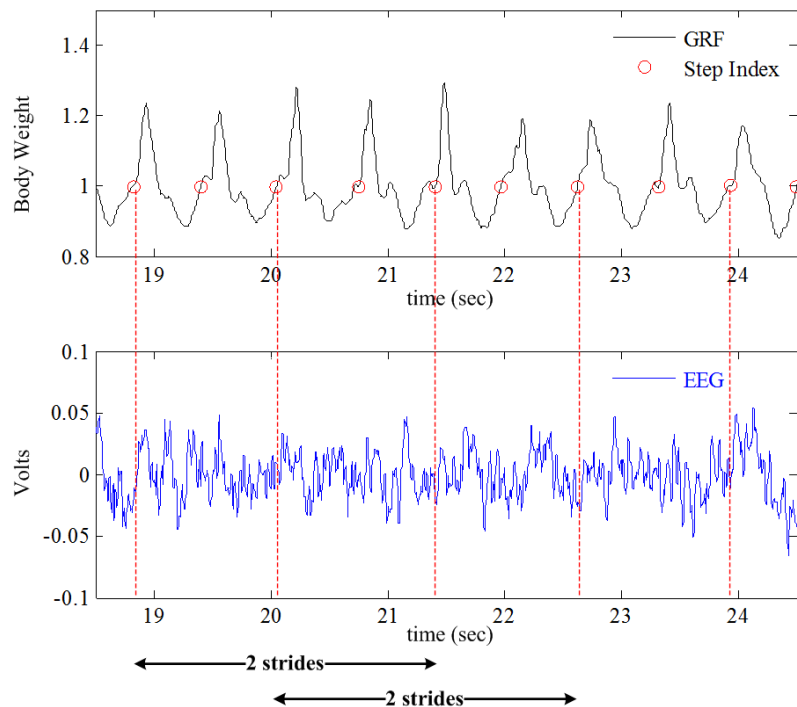


Figure 4-16. Epoch segmentation in walking condition

Although independent component analysis is a good tool for separating artifact and EEG signals, some ‘odd’ epochs remain in the data. So, we used a statistical artifact removal approach to delete these ‘odd’ epochs; the detailed process is shown in Figure 4-17. The detail will be introduced in Section 4.5.2 and 4.5.3.

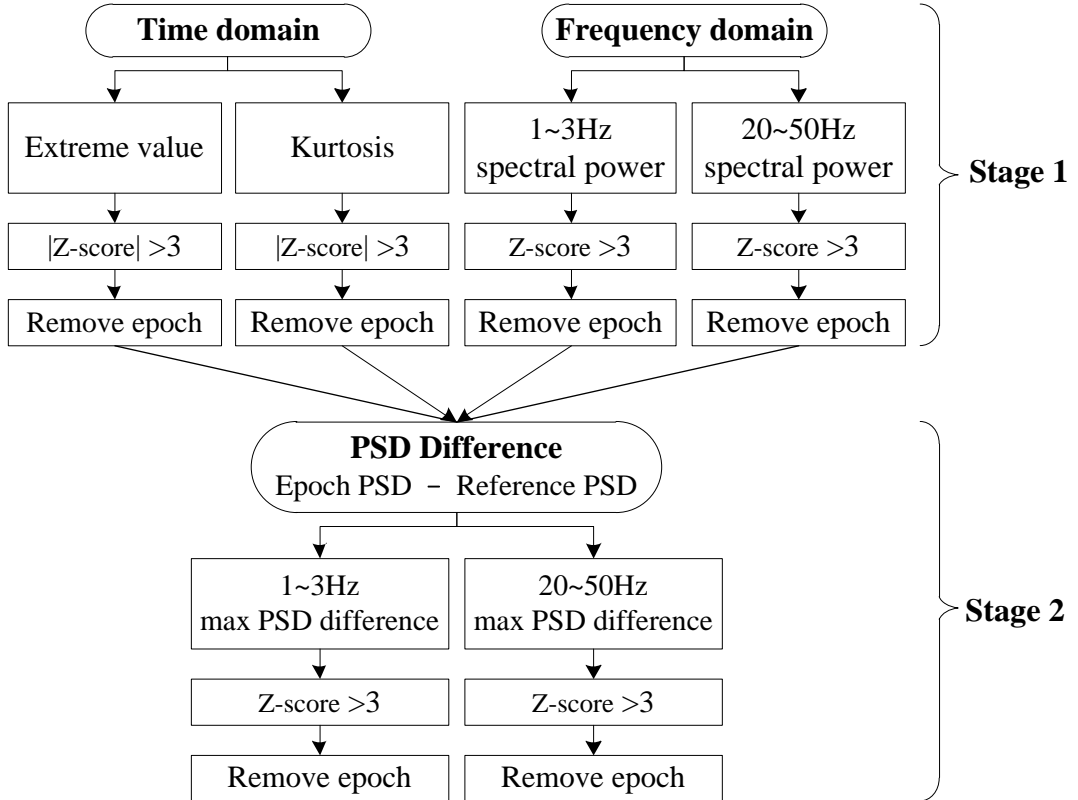


Figure 4-17. Statistical artifact removal process flow

4.5.2 Time-domain statistical analysis

In Figure 4-17, the left portion of the Stage 1 is the time-domain statistical analysis procedure. The epoch segmentation method was introduced in previous section. There are two statistics for epoch rejection criterion: extreme value and kurtosis [38].

Extreme value is very effective for detecting eyes blinking or eyes movement artifacts. We measured the maximum and minimum value in each epoch in order to detect the EOG artifacts.

Kurtosis is a 4th moment statistic which is sensitive to the outliers:

$$K = m_4 - 3m_2^2$$

$$m_n = E\{(x - m_1)^n\}$$

$$m_1 = \text{epoch mean}$$
(4.25)

where m_n is the n^{th} central moment of the epoch, E is an expectation operator. The positive kurtosis is called super-Gaussian distribution. If K is a large positive number, the distribution may be peaked with the muscle activity or small eyes blinking. The negative kurtosis is called sub-Gaussian distribution. In particular, if K is a very negative number, the distribution usually present AC (alternating current) or DC (direct current) artifacts in the epoch. When $K = 0$, the distribution of the epoch is standard Gaussian distribution.

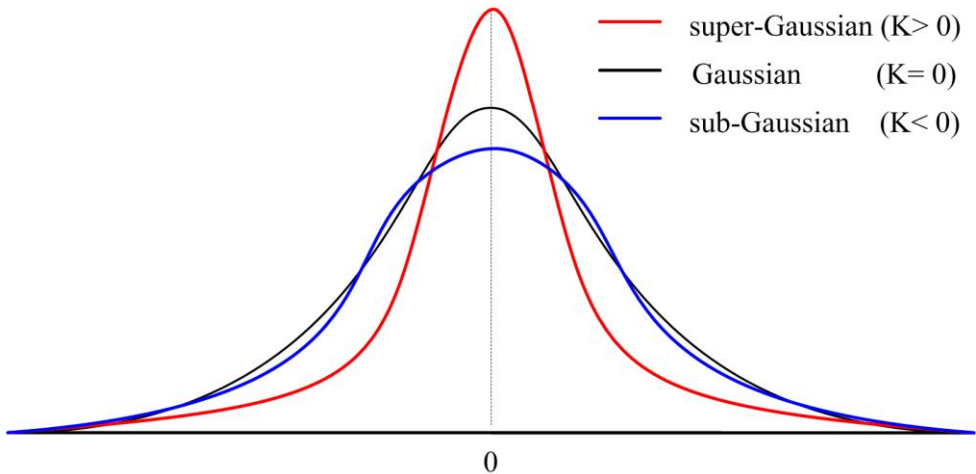


Figure 4-18. PDF shape of super-Gaussian, Gaussian and sub-Gaussian

Then, we normalized these measures by Z-score transform:

$$z = \frac{x - \mu}{\sigma}$$
(4.26)

Where x is the measure of epoch, μ is the mean of the measure, σ is the standard deviation of the measure. If $z > 3$ or $z < -3$, the epoch is considered to be contaminated and will be removed in the data.

4.5.3 Frequency-domain statistical analysis

The right portion of Stage 1 and the Stage 2 are both frequency-domain statistical analysis.

In the right part of Stage 1, each epoch's power spectral density (PSD) was obtained based on the technique illustrated in the previous section and the resulting spectral patterns were used to detect the abnormal epochs. The muscle noise usually induces relatively strong spectral power in 20-50Hz frequency band whereas eyes blinking usually generates relatively strong spectral power in 1-3Hz frequency band. The spectral power of these two frequency bands were transformed to z-score and the epochs when $z\text{-score} > 3$ were removed.

In Stage 2, we compared the spectral differences between each epoch's PSD and the reference PSD. First, the reference PSD was chosen by the ensemble average of the PSDs which were obtained in Stage 1. Next, we subtracted the reference PSD from each epoch's PSD. Next, the maximum differences in 1~3Hz and 20~50Hz frequency bands were determined and transformed to z -score. The epochs whose z -score > 3 were removed.

Chapter 5

EEG Spectral Analysis

This study compares before walking, during walking and after walking EEG signals. Figure 5-1 depicts the arrangement for an experimental trial. The interval between 0.5 minute to 2.5 minute was selected as the baseline (before period in Figure 5-1) of EEG rhythms. The entire walking period was used to estimate the EEG rhythms of the walking process. The first 5 second of the after walking period was not used to allow the treadmill to come to a complete stop. The following 55 seconds of the after walking period was used to compute the after walking EEG rhythms.

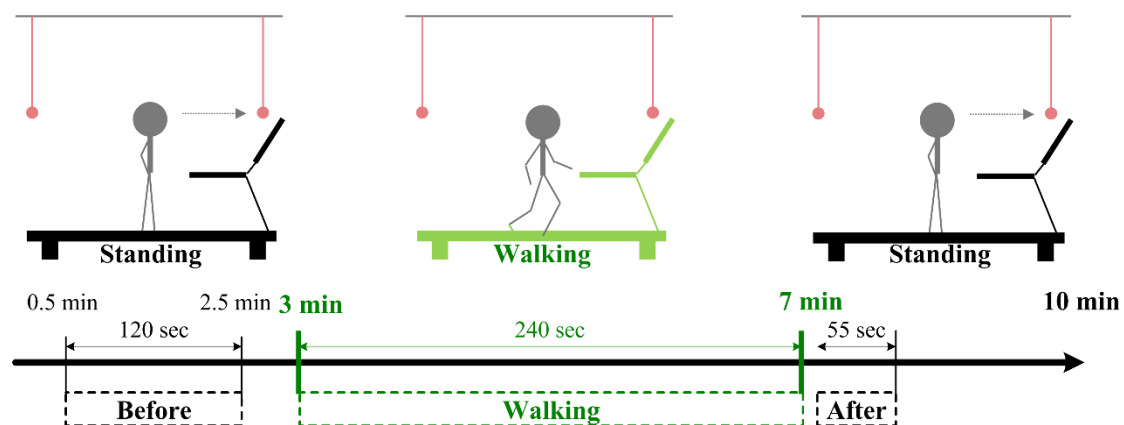


Figure 5-1. Three periods in the experiment

We will compare EEG rhythms and asymmetry between forward and backward walking for before walking, during walking and after walking periods. We will also compare forward and backward walking for the amount of EEG rhythm and asymmetry variations from before walking to after walking periods. These spectral features will be discussed in following sections.

5.1 EEG Power Spectral Density Estimation

The ensemble average of qualified PSDs processed in Chapter 4 was calculated

to estimate the absolute PSD for each EEG channel. Then, the relative PSD, D_r was calculated by:

$$D_r(i) = \frac{D_n(i)}{\sqrt{\sum_{k=1}^{50} D_n^2(k)}}, \quad i = 1, 2, \dots, 50 \quad (5.1)$$

where D_n is the amplitude spectrum at n Hz. Next, to improve normality, the natural logarithmic transform of D_r was used for further processing [39]. The average relative PSD and absolute PSD for the analyzed subjects were shown in Appendix II and Appendix IV respectively.

5.2 EEG Rhythms Analysis

5.2.1 EEG Rhythms

The EEG rhythms were categorized as *Delta* (1-4Hz), *Theta* (4-8Hz), *Alpha* (8-12Hz), *Beta* (12-30Hz), β_3 (30-40Hz) and *Gamma* (40-50Hz). *Alpha* rhythm can be divided into two sub-bands: α_1 (8-10Hz) and α_2 (10-12Hz), *Beta* rhythm can be split into three sub-bands: σ (12-15Hz), β_1 (15-18Hz) and β_2 (18-30Hz), as illustrated in Figure 5-2:

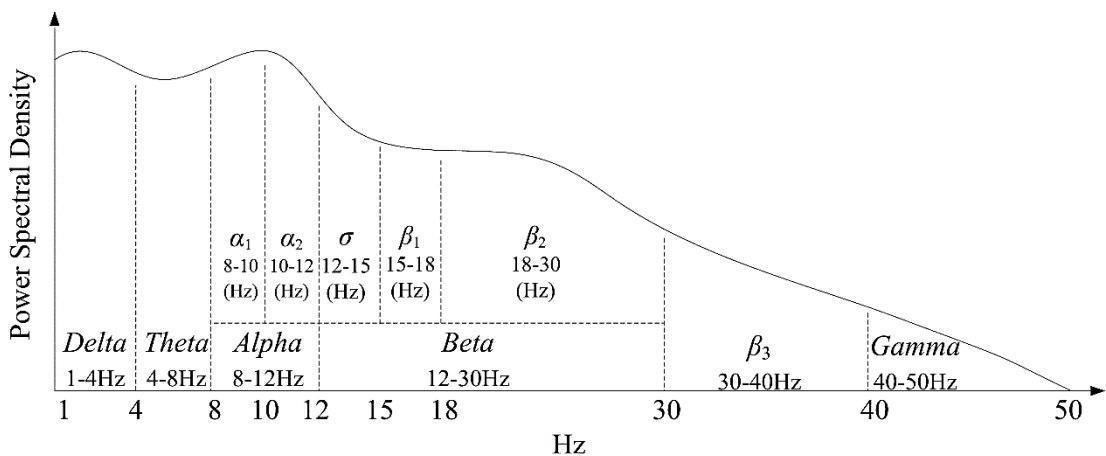


Figure 5-2 EEG Rhythms and frequency bands

The relative rhythmic power R_r were calculated by Equation 5.2:

$$R_r(i) = \frac{R_a(i)}{\sqrt{\sum_{k=1}^6 R_m^2(k)}}, \quad i = 1, 2, \dots, 11 \quad (5.2)$$

where R_a was the absolute rhythmic power, R_m was the absolute rhythmic power that includes *Delta*, *Theta*, *Alpha*, *Beta*, β_3 and *Gamma* rhythms. Next, a natural logarithmic transform of the relative rhythmic power was applied to stabilize the variances [40].

5.2.2 EEG Rhythm Increment

EEG rhythm increment was calculated by the following equation:

$$\log A - \log B \quad (5.3)$$

where \log is the natural logarithmic transform operator, A is the relative rhythmic power after walking and B is the relative rhythmic power before walking.

5.2.3 EEG Rhythm Asymmetry

EEG asymmetry was calculated by the following equation:

$$\log R - \log L \quad (5.4)$$

where R is the relative rhythmic power on right hemisphere, L is the relative rhythmic power on left hemisphere.

5.3 Statistical Hypothesis Test

Statistical hypothesis test is an inference method used for making decision from the sampled data.

In hypothesis for a population parameter μ , the sample parameter μ_0 , is used to test the hypothesis under two conditions. One is the null hypothesis, which is denoted by H_0 , and assuming the sample parameter μ_0 is equal to population parameter μ ($\mu = \mu_0$). The other is the alternative hypothesis, which is denoted by H_a , and assuming the sample parameter μ_0 isn't equal to population parameter μ ($\mu \neq \mu_0$). Generally, the

unwanted results are usually set as the null hypothesis, and the event which we want to prove are usually set as alternative hypothesis.

The above hypothesis test is a two-tailed test because the rejection region is located in the upper tail and lower tail of sampling distribution (see Figure 5-3).

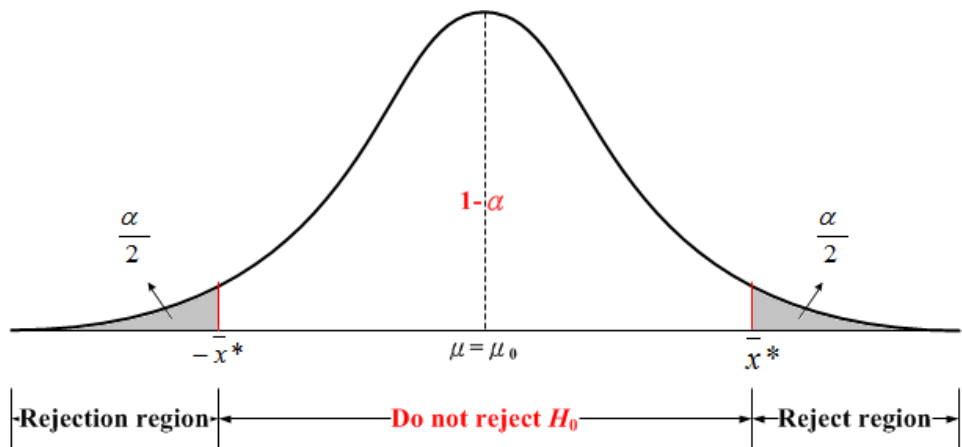


Figure 5-3. Two-tail hypothesis test

The area of the reject region gives the probability of getting μ isn't equal to μ_0 when μ is really equal to μ_0 , and it is the probability of making a Type I error. This probability is called the significance level of the test and is denoted by α . The value of α is determined and based on the cost involved in committing a Type I error.

However, there is another type of decision error: Type II error. Type II error is an incorrect decision which accept a false null hypothesis. The relationship between decision and real state was showed in Table 5-1.

Table 5-1. Type I error and Type II error

	H_0 is true	H_0 is false
Accept H_0	Correct Decision	Type II error
Reject H_0	Type I error	Correct Decision

The probability of Type II error is denoted by β , which is inversely related to α . So, it's important to consider both sides of the issue in setting α . When α is chosen,

the critical value $\pm \bar{x}^*$ could be calculated by t -distribution.

5.3.1 Hypothesis Tests for Dependent Samples

Dependent samples (paired samples) can be used to control for an outside source of variation. For example, in this thesis, we want to estimate the EEG rhythms difference between forward walking and backward walking. Because the same subjects tested both types of walking directions with the same speed (3km/h), the EEG measures will most likely be related. The two samples are not independent, but are instead considered dependent samples.

The dependent test statistics are computed using Eq. (5.5):

$$t^* = \frac{\bar{d} - \mu_d}{\frac{s_d}{\sqrt{n}}}, \quad df = (n-1) \quad (5.5)$$

Where:

$$\bar{d} = \text{Mean paired difference} = \frac{\sum d}{n}$$

μ_d = Hypothesized population mean paired difference

$$s_d = \text{Sample standard deviation for paired difference} = \sqrt{\frac{\sum (d - \bar{d})^2}{n-1}}$$

n = Number of paired values in the sample

The null and alternative are:

$$\begin{aligned} H_0 : \mu_d &= 0 \\ H_A : \mu_d &\neq 0 \end{aligned} \quad (5.6)$$

The t^* score could be transformed to p -value. If p -value $< \alpha$, the two samples are considered a significant difference. And the greater $|t^*|$ (or the smaller p -value), the more significant difference between two samples.

Based upon these spectral features and dependent test, the difference between forward walking and backward walking will be discussed in next chapter.

Chapter 6

Experimental Result

6.1 Performance of Gait-related Artifact Removal

A previous study compared the spectral power of the 1.5 to 8.5Hz frequency band to assess the efficacy of gait-related removal method [27]. Another study demonstrated that the same harmonics were found in the EEG and GRF spectra during gait motion and thus characterized the motion artifacts removal performance by the amount of reduction of the harmonics amplitudes [29].

According to these studies, we introduced the spectral power ratio (*SPR*) and mode power ratio (*MPR*) in order to evaluate the adaptive filter performance.

6.1.1 Spectral Power Ratio

The spectral power was calculated by:

$$\text{Spectral Power Ratio} = \frac{\text{Filtered EEG } 1.5\text{Hz} \sim 8.5\text{Hz spectral power}}{\text{Raw EEG } 1.5\text{Hz} \sim 8.5\text{Hz spectral power}} \quad (6.1)$$

where the *Raw EEG* data was the EEG data that was only corrected by visual inspection described in Section 4.3. There were two types of *Filtered EEG* data: one was EEG data of Figure 4-1, another was EEG data of Figure 4-1 but without LMS adaptive filter. The ensemble channel-averages for each EEG data were also computed to evaluate the mean power ratio for each subjects.

6.1.2 Mode Power Ratio

As shown in Figure 6-1, the walking GRF is an almost periodic signal. Hence, the signal spectral energy was concentrated in the harmonics.

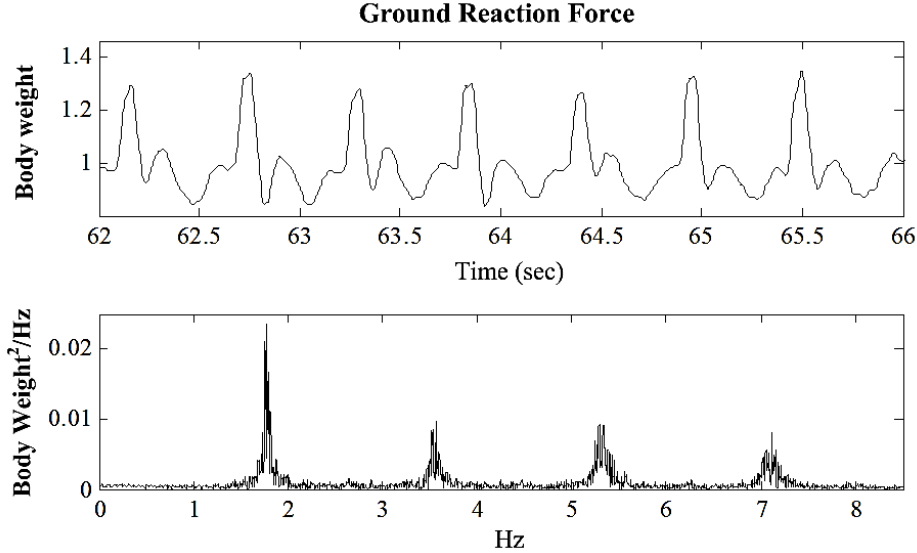


Figure 6-1. GRF signal and spectrum

Since the motion artifact is induced by walking, the most affected frequency bands are supposed to relate to these harmonics. The fundamental frequency of the GRF harmonics in each epoch was largely determined by the time of stride interval. So the PSDs of each epoch will be normalized by fundamental frequency before comparing the mode power.

The GRF and EEG signals were segmented into epochs of 2 stride cycles and overlapped by 1 stride cycle. The spectra of these epochs were computed by FFT after multiplying a Hamming window. The fundamental frequency f_0 was calculated by [41]:

$$f_0 = \frac{1}{T_0} , T_0 = \frac{T_{2\text{stride}}}{4} \quad (6.2)$$

$T_{2\text{stride}}$: epoch length

The signals were padded with tailing zeros to 250 times the length of the epoch. With the frequency resolution f_r and fundamental frequency f_0 we have $f_0 = 1000 f_r$. This equality can be derived from:

$$f_r = \frac{1}{T} = \frac{1}{C \times T_{\text{stride}}} = \frac{1}{4CT_0} = \frac{f_0}{4C} = \frac{f_0}{1000} \quad (6.3)$$

$$\therefore C = 250$$

Finally, we average the theses epochs to estimate the normalized PSD (NPSD). By defining Mode1 corresponds to $0.5f_0 \sim 1.5f_0$, Mode2 corresponds to $1.5f_0 \sim 2.5f_0$, Mode3 corresponds to $2.5f_0 \sim 3.5f_0$ and Mode4 corresponds to $3.5f_0 \sim 4.5f_0$, so for the mode power ratio (*MPR*) was calculated by:

$$\text{Mode Power Ratio} = \frac{\text{Filtered EEG mode power}}{\text{Raw EEG mode power}} \quad (6.4)$$

where the *Raw EEG* data and *Filter EEG* data were the same as Section 6.1.2.

6.1.3 Results

Figure 6-1 and Figure 6-2 give a typical example of the ensemble channel-average PSD and NPSD of one subject. The common gait-related motion harmonics can be observed in EEG PSD before applying the adaptive filtering. As shown in these two figures, the influences of GRF on EEG PSD had been suppressed by the adaptive filter.

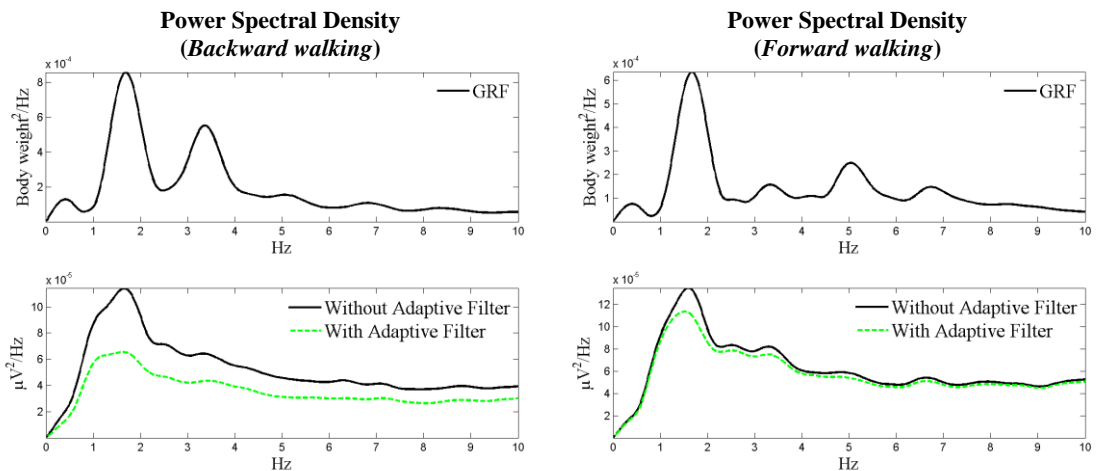


Figure 6-2. Ensemble channel-average PSD (Subject H)

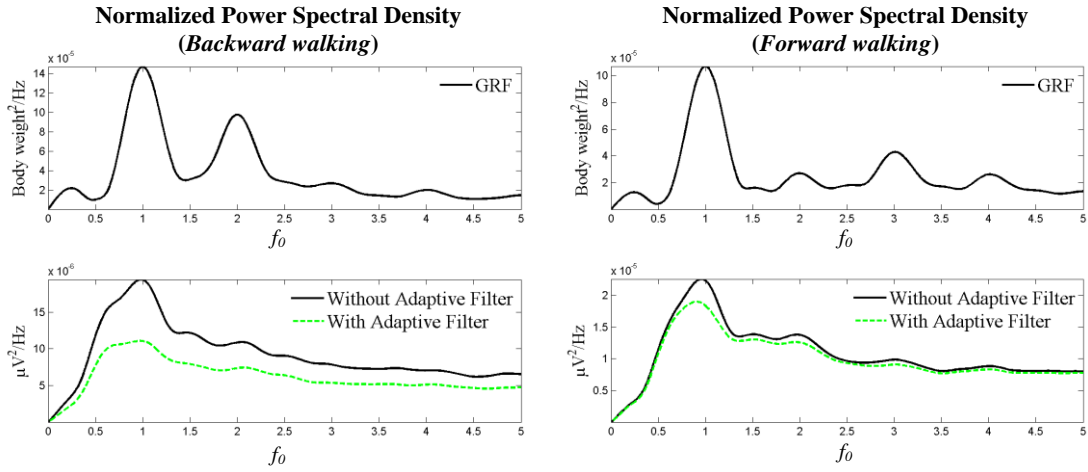


Figure 6-3. Ensemble channel-average NPSD (Subject H)

Dependent *t*-tests show significant decrease on *power ratio* after applying the adaptive filtering process in both forward and backward walking conditions. The corresponding *p*-values and *power ratios* are shown in Table 6-1 and Figure 6-4, respectively.

Table 6-1. Dependent *t*-Test results of power ratios (*p*-value)

<i>p</i> -value	<i>MPR</i>	<i>MPR</i>	<i>MPR</i>	<i>MPR</i>	<i>SPR</i>
	Mode1	Mode2	Mode3	Mode4	1.5~8.5Hz
<i>Forward</i>	0.040	0.014	0.005	0.019	0.034
<i>Backward</i>	0.006	0.013	0.013	0.010	0.007

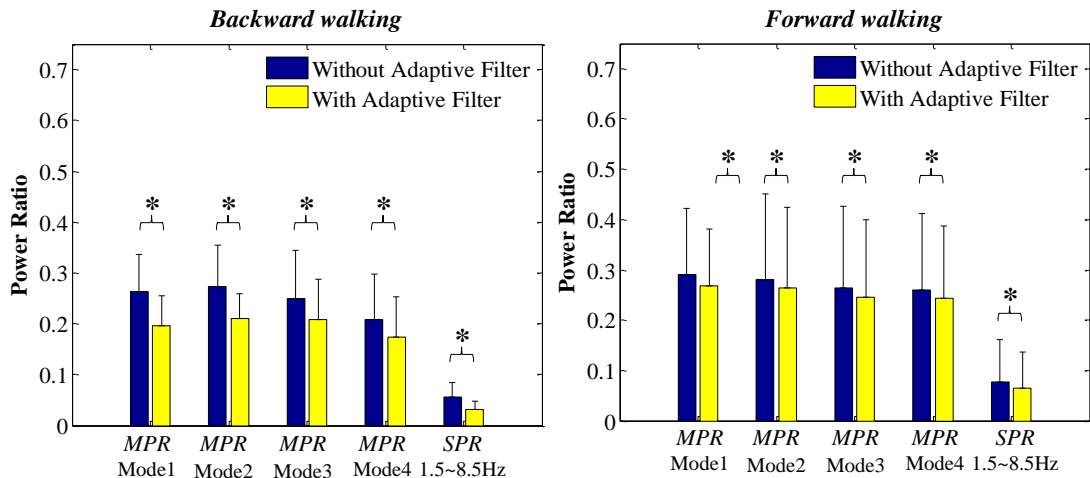


Figure 6-4. The power ratios of EEG data. The star signs indicate the significant (*p*-value < 0.05) difference after applying the adaptive filtering method.

6.2 EEG Rhythm Analysis

19 healthy university students participated in this study. Every subject performed forward and backward walking at 3km/h speed on the force treadmill.

In quiet standing periods (i.e., before and after walking), all the data (19 subjects) were considered reliable and thus used in the analysis. In contrast, only 10 out of the 19 participant's walking period data can be analyzed due to electrode malfunction or poor signal quality. Furthermore, for the walking period, we only studied central and parietal region signals due to the following two reasons: 1) Occipital region are severely contaminated by neck muscles artifacts. 2) Central and parietal region are highly related with sensory and motor functions.

The following sections summarize the dependent *t*-test results with *p*-value tables. Note that the significant level for the statistical difference was set as 0.05. The purple and orange cells in the tables represent *p*-value < 0.05 and 0.05 < *p*-value < 0.1 respectively.

6.2.1 Forward Walking

Relative to the baseline condition (i.e., before walking period), the red (green) numbers in this section's tables represent the increase (decrease) of the rhythm power.

After forward walking, significant decrease of *Alpha* rhythm power was found in the frontal, parietal and occipital regions, as shown in Table 6-2. Furthermore, we observed that α_1 power was significantly decreased on all electrodes.

Table 6-2. EEG activities of forward walking (comparing after to before periods)

<i>p</i> -value	Alpha	α_1	α_2	Beta	σ	β_1	β_2
	8Hz~12Hz	8Hz~10Hz	10Hz~12Hz	12Hz~30Hz	12Hz~15Hz	15Hz~18Hz	18Hz~30Hz
F3	0.004	0.005	0.018	0.395	0.911	0.330	0.168
F4	0.077	0.013	0.573	0.468	0.201	0.948	0.737
C3	0.080	0.040	0.245	0.939	0.234	0.122	0.182
C4	0.152	0.012	0.619	0.776	0.224	0.168	0.405
P3	0.011	0.020	0.016	0.356	0.775	0.221	0.225
P4	0.007	0.003	0.023	0.395	0.674	0.102	0.379
O1	0.021	0.004	0.098	0.138	0.601	0.058	0.120
O2	0.023	0.001	0.240	0.181	0.612	0.071	0.191

In Table 6-3, the significant decrease of *Alpha* and *Beta* rhythm power in the central and parietal cortex were found during walking. In addition, such decrease are mainly contributed by the variation of the α_2 , σ and β_1 power (10-18Hz).

Table 6-3. EEG activities of forward walking (comparing during to before periods)

<i>p</i> -value	Alpha	α_1	α_2	Beta	σ	β_1	β_2
	8Hz~12Hz	8Hz~10Hz	10Hz~12Hz	12Hz~30Hz	12Hz~15Hz	15Hz~18Hz	18Hz~30Hz
C3	0.011	0.272	0.005	0.003	0.000	0.016	0.076
C4	0.000	0.032	0.000	0.000	0.001	0.019	0.010
P3	0.003	0.018	0.001	0.002	0.001	0.002	0.070
P4	0.014	0.083	0.005	0.010	0.002	0.017	0.090

6.2.2 Backward Walking

After backward walking, the *Alpha* power was significantly decreased in central and parietal cortex. Compared to the results of Table 6-2 of forward walking, the central and occipital regions have different variation patterns in backward walking. In central region, both α_1 and α_2 power decreased after backward walking. In comparison, only α_1 decreased after forward walking. In occipital region, α_1 rhythm showed a significant decrease in both occipital electrodes after forward walking but such a decrease only appear in O1 electrode for backward walking.

Table 6-4. EEG activities of backward walking (comparing after to before periods)

p-value	Alpha			Beta			
	α_1 8Hz~12Hz	α_2 8Hz~10Hz	α_2 10Hz~12Hz	σ 12Hz~30Hz	β_1 12Hz~15Hz	β_2 15Hz~18Hz	β_2 18Hz~30Hz
F3	0.092	0.181	0.091	0.240	0.393	0.302	0.233
F4	0.019	0.002	0.169	0.196	0.341	0.119	0.038
C3	0.006	0.009	0.012	0.814	0.595	0.314	0.403
C4	0.001	0.002	0.006	0.654	0.853	0.865	0.136
P3	0.001	0.000	0.007	0.738	0.654	0.498	0.203
P4	0.045	0.083	0.048	0.575	0.613	0.636	0.262
O1	0.044	0.042	0.069	0.333	0.939	0.171	0.101
O2	0.288	0.474	0.296	0.909	0.068	0.545	0.230

As shown in Table 6-5, the rhythm power of the *Alpha* and *Beta* in central and parietal regions were significantly decreased during backward walking. In comparison, for backward walking, a decrease are mainly contributed by the variation of the α_2 and σ (10-15Hz).

Table 6-5. EEG activities of backward walking (comparing during to before periods)

p-value	Alpha			Beta			
	α_1 8Hz~12Hz	α_2 8Hz~10Hz	α_2 10Hz~12Hz	σ 12Hz~30Hz	β_1 12Hz~15Hz	β_2 15Hz~18Hz	β_2 18Hz~30Hz
C3	0.001	0.065	0.000	0.004	0.000	0.057	0.042
C4	0.000	0.123	0.000	0.001	0.000	0.115	0.054
P3	0.000	0.006	0.000	0.074	0.013	0.086	0.177
P4	0.002	0.033	0.001	0.017	0.002	0.024	0.095

6.2.3 Forward Walking versus Backward Walking

In this Section, forward walking condition was set as the baseline. Therefore, in the *p*-value tables, the red (green) numbers indicated that backward walking has a larger (smaller) power than forward walking.

As shown in Table 6-6, in before-walking period, backward walking results in larger *Beta* power in frontal cortex, particularly in the right frontal region (F4).

Table 6-6. EEG activities of the before walking period (comparing backward to forward)

p-value	Alpha		α_1	α_2	Beta		σ	β_1	β_2
	8Hz~12Hz	8Hz~10Hz	10Hz~12Hz	12Hz~30Hz	12Hz~15Hz	15Hz~18Hz	18Hz~30Hz		
F3	0.536	0.474	0.678	0.129	0.323	0.076	0.095		
F4	0.923	0.480	0.255	0.005	0.007	0.032	0.009		
C3	0.213	0.960	0.103	0.388	0.390	0.367	0.559		
C4	0.143	0.634	0.013	0.079	0.078	0.447	0.261		
P3	0.052	0.630	0.022	0.427	0.598	0.873	0.053		
P4	0.931	0.557	0.464	0.183	0.062	0.386	0.291		
O1	0.731	0.480	0.224	0.719	0.168	0.767	0.296		
O2	0.726	0.126	0.336	0.622	0.273	0.555	0.260		

As shown by the after walking results summarized in Table 6-7, backward walking has larger β_1 power in the central region. On the other hand, the *Alpha* power has opposite trend on the same region (central), but has not reached statistical significance.

Table 6-7. EEG activities of the after walking period (comparing backward to forward)

p-value	Alpha		α_1	α_2	Beta		σ	β_1	β_2
	8Hz~12Hz	8Hz~10Hz	10Hz~12Hz	12Hz~30Hz	12Hz~15Hz	15Hz~18Hz	18Hz~30Hz		
F3	0.365	0.275	0.608	0.106	0.626	0.129	0.087		
F4	0.943	0.796	0.896	0.302	0.062	0.335	0.694		
C3	0.167	0.395	0.180	0.267	0.378	0.055	0.374		
C4	0.161	0.614	0.186	0.786	0.713	0.020	0.913		
P3	0.579	0.876	0.526	0.657	0.284	0.503	0.387		
P4	0.520	0.325	0.993	0.137	0.213	0.080	0.381		
O1	0.722	0.780	0.708	0.889	0.215	0.415	0.290		
O2	0.088	0.045	0.235	0.212	0.010	0.186	0.596		

After walking, Table 6-8 shows that backward walking has significantly lower *Alpha* power increment in central region as compared to forward walking. Based on the results of Table 6-2 and 6-4, we can infer that *Alpha* power increment is negative in both forward and backward walking conditions. As a consequence, the results of Table 6-8 indicate that backward walking yields greater suppression on *Alpha* power

in after-walking period than forward mode.

Table 6-8. EEG increment after walking (comparing backward to forward)

<i>p</i> -value	<i>Alpha</i>			<i>Beta</i>			
	α_1 8Hz~12Hz	α_2 8Hz~10Hz	10Hz~12Hz	σ 12Hz~30Hz	β_1 12Hz~15Hz	15Hz~18Hz	β_2 18Hz~30Hz
F3	0.260	0.173	0.516	0.963	0.643	0.743	1.000
F4	0.996	0.630	0.626	0.068	0.551	0.266	0.027
C3	0.032	0.436	0.026	0.820	0.863	0.092	0.968
C4	0.018	0.941	0.009	0.289	0.118	0.219	0.434
P3	0.572	0.678	0.510	0.469	0.497	0.544	0.903
P4	0.561	0.099	0.544	0.648	0.908	0.152	0.908
O1	0.976	0.384	0.595	0.660	0.708	0.423	0.871
O2	0.110	0.003	0.782	0.117	0.044	0.060	0.731

The results of Table 6-9 shows that, during walking, the α_2 and σ power of the central region subject to greater suppression in backward walking. It should be noted that the frequency band of σ rhythm is the same as the frequency band of sensorimotor rhythm (SMR). Generally speaking, stronger SMR corresponds to the idling of sensory-motor areas. That is, activation of sensorimotor areas typically results in the decrease of SMR power [42].

Table 6-9. EEG activities of the during walking periods (comparing backward to forward)

<i>p</i> -value	<i>Alpha</i>			<i>Beta</i>			
	α_1 8Hz~12Hz	α_2 8Hz~10Hz	10Hz~12Hz	σ 12Hz~30Hz	β_1 12Hz~15Hz	15Hz~18Hz	β_2 18Hz~30Hz
C3	0.103	0.233	0.043	0.070	0.033	0.174	0.126
C4	0.177	0.740	0.024	0.142	0.003	0.584	0.507
P3	0.148	0.187	0.122	0.372	0.587	0.410	0.284
P4	0.275	0.430	0.162	0.587	0.634	0.711	0.600

As shown by Table 6-10, during walking, backward walking has significant smaller *Alpha* power increment in central region. Since we have negative rhythm in both walking modes, such a result implies that the backward walking has stronger desynchronization on *Alpha* power than forward walking. Table 6-10 also shows that

in the central region, backward walking has smaller increment in the 10Hz to 15Hz (α_2 and σ rhythms).

Table 6-10. EEG increment during walking (comparing backward to forward)

p-value	Alpha			Beta			
	8Hz~12Hz	α_1	α_2	12Hz~30Hz	σ	β_1	β_2
C3	0.090	0.197	0.047	0.237	0.124	0.496	0.232
C4	0.020	0.812	0.001	0.121	0.006	0.417	0.378
P3	0.097	0.216	0.055	0.438	0.471	0.614	0.377
P4	0.213	0.455	0.107	0.265	0.193	0.425	0.351

6.3 EEG Asymmetry Analysis

6.3.1 Forward Walking

After comparing the EEG spectra before and after forward walking, the results of Table 6-11 shows that forward walking increases of α_2 and *Beta* power asymmetry in frontal region. However, such increases are not statistically significant. Compared with the before-walking period, no change can be detected during forward walking period.

Table 6-11. EEG asymmetry on forward walking (after versus before walking)

p-value	Alpha			Beta			
	8Hz~12Hz	α_1	α_2	12Hz~30Hz	σ	β_1	β_2
Frontal	0.124	0.534	0.070	0.065	0.199	0.212	0.159
Central	0.775	0.412	0.452	0.833	0.777	0.873	0.867
Parietal	0.744	0.175	0.814	0.869	0.839	0.530	0.685
Occipital	0.722	0.115	0.547	0.908	0.989	0.989	0.830

Table 6-12. EEG asymmetry on forward walking (during versus before walking)

p-value	Alpha			Beta			
	8Hz~12Hz	α_1	α_2	12Hz~30Hz	σ	β_1	β_2
Central	0.375	0.229	0.728	0.626	0.562	0.514	0.567
Parietal	0.915	0.927	0.861	0.782	0.926	0.938	0.655

6.3.2 Backward Walking

From Table 6-13, it is found that the after walking period σ rhythm asymmetry in frontal region is significantly larger than that of before walking periods. In addition, such a significant asymmetry increase also appear in the α_1 band for the occipital region. As demonstrated by the results of Table 6-14, after comparing the EEG spectra of the before-walking and during-walking periods, we can detect any significant differences for backward walking.

Table 6-13. EEG asymmetry on backward walking (comparing after to before periods)

p-value	Alpha			Beta			
	8Hz~12Hz	α_1	α_2	12Hz~30Hz	σ	β_1	β_2
Frontal	0.993	0.162	0.380	0.981	0.031	0.332	0.235
Central	0.845	0.931	0.990	0.516	0.210	0.391	0.757
Parietal	0.256	0.094	0.798	0.740	0.197	0.518	0.891
Occipital	0.097	0.046	0.187	0.165	0.067	0.302	0.384

Table 6-14. EEG asymmetry on backward walking (comparing during to before periods)

p-value	Alpha			Beta			
	8Hz~12Hz	α_1	α_2	12Hz~30Hz	σ	β_1	β_2
Central	0.420	0.163	0.499	0.858	0.573	0.741	0.393
Parietal	0.712	0.588	0.859	0.990	0.674	0.901	0.701

6.3.3 Forward Walking versus Backward Walking

Table 6-15 and Table 6-16 summarize the comparative forward versus backward EEG asymmetry results for the before-walking periods and after-walking periods, respectively. As shown in Table 6-15, in before-walking period, backward walking results in lower asymmetry *Beta* activity in the central region. For the after walking periods, as shown by Table 6-16, such a difference appear in the occipital region. For the during-walking period, as demonstrated by Table 6-17, no significant difference

can be found between forward and backward walking EEG asymmetry.

Table 6-15. EEG asymmetry before walking (comparing backward to forward)

<i>p</i> -value	<i>Alpha</i>			<i>Beta</i>			
	α_1 8Hz~12Hz	α_2 8Hz~10Hz	α_2 10Hz~12Hz	σ 12Hz~30Hz	σ 12Hz~15Hz	β_1 15Hz~18Hz	β_2 18Hz~30Hz
Frontal	0.380	0.773	0.224	0.183	0.190	0.288	0.642
Central	0.715	0.325	0.389	0.087	0.040	0.106	0.208
Parietal	0.379	0.291	0.551	0.177	0.193	0.415	0.100
Occipital	0.306	0.190	0.482	0.953	0.502	0.736	0.822

Table 6-16. EEG asymmetry after walking (comparing backward to forward)

<i>p</i> -value	<i>Alpha</i>			<i>Beta</i>			
	α_1 8Hz~12Hz	α_2 8Hz~10Hz	α_2 10Hz~12Hz	σ 12Hz~30Hz	σ 12Hz~15Hz	β_1 15Hz~18Hz	β_2 18Hz~30Hz
Frontal	0.389	0.149	0.717	0.376	0.148	0.395	0.061
Central	0.826	0.681	0.910	0.193	0.304	0.377	0.224
Parietal	0.792	0.245	0.576	0.214	0.569	0.186	0.127
Occipital	0.250	0.055	0.548	0.082	0.036	0.368	0.296

Table 6-17. EEG asymmetry during walking (comparing backward to forward)

<i>p</i> -value	<i>Alpha</i>			<i>Beta</i>			
	α_1 8Hz~12Hz	α_2 8Hz~10Hz	α_2 10Hz~12Hz	σ 12Hz~30Hz	σ 12Hz~15Hz	β_1 15Hz~18Hz	β_2 18Hz~30Hz
Central	0.221	0.148	0.316	0.528	0.705	0.341	0.289
Parietal	0.876	0.701	0.969	0.408	0.775	0.363	0.230

Chapter 7

Discussion and Future Works

7.1 Performance of Gait-related Artifacts Removal

For gait-related artifacts removal, we employed two criteria (*MPR* and *SPR*) to evaluate the performance of adaptive filter performance. In Figure 6-1, we discover that the mode power ratio is the better criterion since the frequency band associated with the spectral power ratio (1.5-8.5Hz) does not cover the entire contaminated frequency band. In particular, it is found that the frequencies band from 1Hz to 0.5Hz was severely contaminated by the harmonics of the motion-induced noise.

Although significant decrease on power ratio can be found in both forward and backward walking modes, our results show that adaptive filtering performs relatively poorly for forward walking. The results summarized in Appendix I demonstrate the differences of spectral pattern between forward and backward walking on GRF signal. In specific, the backward walking has relatively large amplitude in Mode1 and Mode2, and its spectral energy are relatively concentrated in Model and Mode2. This property can be verified by the GRF bandwidth (90% signal energy) results of Table 7-1 and the results of GRF fundamental frequencies (f_0) summarized in Table 7-2:

Bandwidth	<i>Forward</i>	<i>Backward</i>
Mean	6.09	4.70
Std.	0.86	0.99
<i>p</i> -value	7.17E-04	

Table 7-1 GRF Bandwidth (unit: Hz)

f_0	<i>Forward</i>	<i>Backward</i>
Mean	1.62	1.79
Std.	0.09	0.16
<i>p</i> -value	5.43E-03	

Table 7-2. GRF f_0 (unit: Hz)

Table 7-1 and Table 7-2 show that the backward walking GRF bandwidth is significantly lower than forward walking (p -value<0.05) but f_0 is significantly higher

than forward walking (p -value<0.05). Moreover, in backward walking, the GRF bandwidth was lower than f_2 (three times of f_0); on the other hand, in forward walking, the GRF bandwidth was higher than f_2 . Therefore, we suggest that the relation between GRF features and gait-related artifacts should be more thoroughly studied in the future.

7.2 Different EEG Patterns in Forward and Backward Walking

In the before-walking period, backward walking yields higher *Beta* activity in frontal region. The frontal *Beta* activity was identified as the background activities in tense and anxious condition [43]. Therefore, this result seems to suggest that the tested subjects were in a relatively stressed condition before backward walking which is an unfamiliar locomotion mode for most of us.

In the during-walking period, our EEG rhythm experimental results are in agreement with previous studies for both forward and backward walking modes. In specific, the power of *Alpha* and *Beta* rhythms become smaller in both walking modes. However, the desynchronization of *Alpha* band power is more significant in backward walking. Previous studies also suggested that the less automatic movements leads the more desynchronization [15]. This results may be related to a greater demand for the integration of motor and sensory information in the sensorimotor cortex.

Additionally, in EEG activity and EEG increment analysis (Table 6-9 and Table 6-10), backward walking showed a significantly more suppression than forward walking for both α_2 and σ rhythm. The previous studies suggested that the decreased parietal α_2 power is associated to the increased somatosensory information processing [48 49 50]. For σ rhythm (i.e. sensorimotor rhythm, SMR), backward walking showed a stronger SMR suppression in central region, it might be related to an increase of the somatosensory inputs [42]. In view of the above, the backward walking involve more

sensorimotor cortex activities and provides more sensorimotor training than forward walking.

In this study, after walking, the *Alpha* rhythm demonstrated significant decrease in both walking modes. These results are inconsistent with most of the previous studies [44]. In previous studies, *Alpha* rhythm actually increases after exercises. *Alpha* rhythm reduction has been associated with fatigue or relaxation conditions. It has been reported that certain level of intensity is needed to evoke exercise-related EEG changes and the suggested threshold is between 50% and 80% of the individual capacity [17]. We can estimate the exercise intensity by [45]:

$$\text{Exercise intensity} = \text{heart rate} / (220 - \text{age}) * 100\% \quad (7.1)$$

Since the ages of these subjects vary from 22 to 31, therefore the heart rate that associated with the suggested lower threshold (50%) ranges from 95bpm to 99bpm. The median heart rate during walking period were showed in the Table 7-3:

Heart Rate	<i>Forward</i>	<i>Backward</i>
Mean	92.16	103.25
Std.	9.08	11.56
<i>p</i> -value	4.86E-08	

Table 7-3. Median heart rate during walking (unit: bpm)

Although the backward walking is a relatively higher intensity exercise when compared to forward walking, it still did not reach the suggested lower threshold. Therefore, our experimental results might not be the exercise induced response. We speculate that the *Alpha* desynchronization might be related to a state of tension. The experimental protocol required the subjects to keep the eyes on the tennis ball after walking, so, the subjects were in an ‘eyes open’ condition and still paid attention to the instruction. Additionally, this ‘eyes open’ condition was different from most of the previous studies [44], it may thus influence the experimental results.

The EEG asymmetry of *Alpha* power in frontal and parietal locations has been extensively interpreted [46]. However, as shown in Section 6.3, there is no significant asymmetry change in *Alpha* rhythm in frontal and parietal region. There are several studies reported that the EEG asymmetry cannot predict affective response at low exercise intensity [47], and this may be the reason why we cannot find significant asymmetry changes. However, we can still identify different asymmetry patterns between two walking modes, especially for the α_1 and σ rhythms.

This study has compared different EEG spectral features between the forward and backward walking and has provided some neurological supports for backward walking training. These comparative results may be valuable for the ambulatory brain-computer interface (BCI) system employed during rehabilitation process.

Reference

1. 張耿維，2014，跑步機背向行走訓練對慢性中風患者平衡能力、走路表現與心肺適能之療效，碩士論文，高雄醫學大學運動醫學研究所。
2. Grasso R, Bianchi L, Lacquaniti F. Motor patterns for human gait: backward versus forward locomotion. *J Neurophysiol.* 1998;80(4):1868-85.
3. Winter DA, Pluck N, Yang JF. Backward walking: a simple reversal of forward walking? *J Mot Behav.* 1989;21(3):291-305.
4. Hao WY, Chen Y. Backward walking training improves balance in school-aged boys. *Sports Med Arthrosc Rehabil Ther Technol.* 2011;3:24.
5. Cipriani DJ, Armstrong CW, Gaul S. Backward walking at three levels of treadmill inclination: an electromyographic and kinematic analysis. *J Orthop Sports Phys Ther.* 1995;22(3):95-102.
6. Flynn TW, Soutas-Little RW. Mechanical power and muscle action during forward and backward running. *J Orthop Sports Phys Ther.* 1993;17(2):108-12.
7. Flynn TW, Soutas-Little RW. Patellofemoral joint compressive forces in forward and backward running. *J Orthop Sports Phys Ther.* 1995;21(5):277-82.
8. Drew T, Marigold DS. Taking the next step: cortical contributions to the control of locomotion. *Curr Opin Neurobiol.* 2015;33C:25-33.
9. Luft AR, Smith GV, Forrester L, Whitall J, Macko RF, Hauser TK, Goldberg AP, Hanley DF. Comparing brain activation associated with isolated upper and lower limb movement across corresponding joints. *Hum Brain Mapp.* 2002;17(2):131-40.
10. Dobkin BH, Firestone A, West M, Saremi K, Woods R. Ankle dorsiflexion as an fMRI paradigm to assay motor control for walking during rehabilitation.

Neuroimage. 2004;23(1):370-81.

11. Suzuki M, Miyai I, Ono T, Kubota K. Activities in the frontal cortex and gait performance are modulated by preparation. An fNIRS study. *Neuroimage.* 2008;39(2):600-7.
12. Harada T, Miyai I, Suzuki M, Kubota K. Gait capacity affects cortical activation patterns related to speed control in the elderly. *Exp Brain Res.* 2009;193(3):445-54.
13. Severens M, Nienhuis B, Desain P, Duysens J. Feasibility of measuring Event Related Desynchronization with EEG during walking. *Conf Proc IEEE Eng Med Biol Soc.* 2012;2012:2764-7.
14. Perusquia Hernandez M. A Brain Computer Interface for walking using EEG. Master thesis. Eindhoven University of Technology. 2012.
15. Perusquia Hernandez M. Sensorimotor cortical activity during human gait: Forward and backward walking. Research project. Eindhoven University of Technology. 2012.
16. Pfurtscheller G, Lopes da Silva FH. Event-related EEG/MEG synchronization and desynchronization: basic principles. *Clin Neurophysiol.* 1999;110(11):1842-57.
17. Brümmer V, Schneider S, Abel T, Vogt T, Strüder HK. Brain cortical activity is influenced by exercise mode and intensity. *Med Sci Sports Exerc.* 2011;43(10):1863-72.
18. Harmon-Jones E, Gable PA, Peterson CK. The role of asymmetric frontal cortical activity in emotion-related phenomena. A review and update. *Biol Psychol.* 2010;84(3):451-62.
19. Harmon-Jones E, Harmon-Jones C, Price TF. What is approach motivation? *Emotion Review.* 2013; 5(3):291-295.

20. Hall EE, Ekkekakis P, Petruzzello SJ. Predicting affective responses to exercise using resting EEG frontal asymmetry: Does intensity matter? *Biol Psychol.* 2010;83(3):201-6.
21. Petruzzello SJ, Hall EE, Ekkekakis P. Regional brain activation as a biological marker of affective responsiveness to acute exercise: Influence of fitness. *Psychophysiology.* 2001;38(1):99-106.
22. Hall EE, Ekkekakis P, Petruzzello SJ. Regional brain activity and strenuous exercise. Predicting affective responses using EEG asymmetry. *Biol Psychol.* 2007;75(2):194-200.
23. Vogt T, Schneider S, Brümmer V, Strüder HK. Frontal EEG asymmetry-The effects of sustained walking in the elderly. *Neurosci Lett.* 2010;485(2):134-7.
24. Goncharova II, McFarland DJ, Vaughan TM, Wolpaw JR. EMG contamination of EEG: spectral and topographical characteristics. *Clin Neurophysiol.* 2003;114(9):1580-93
25. Jung TP, Makeig S, Humphries C, Lee TW, McKeown MJ, Iragui V, Sejnowski TJ. Removing electroencephalographic artifacts by blind source separation. *Psychophysiology.* 2000;37(2):163-78.
26. SE. Kerick, KS. Oie, K. McDowell. Assessment of EEG signal quality in motion environments. Army Res. Lab., Rep. ARL-TR-4866. 2009.
27. Gwin JT, Gramann K, Makeig S, Ferris DP. Removal of movement artifact from high-density EEG recorded during walking and running. *J Neurophysiol.* 2010;103(6):3526-34.
28. Gwin JT, Gramann K, Makeig S, Ferris DP. Electrocortical activity is coupled to gait cycle phase during treadmill walking. *Neuroimage.* 2011;54(2):1289-96.
29. T Castermans, M Duvinage, M Petieau, T Hoellinger, C D Saedeleer, K Seetharaman, A Bengoetxea, G Cheron, T Dutoit. Optimizing the performances

- of a P300-based brain–computer interface in ambulatory conditions. *IEEE J. Emerg. Sel. Topics Circuits Syst.* 2011;1(4):566-577.
30. M Duvinage, T Castermans, M Petieau, G Cheron, T Dutoit. Are current gait-related artifact removal techniques useful for low-complexity BCIs?. *IJCNN*. 2012; 1-7.
31. 黃融緯、李懿軒、蔡瀛慶、洪志遠、嚴成文，整合於跑步機地面反作用力的量測裝置，中國機械工程學會第三十一屆全國學術研討會。Taichung, Taiwan, Dec. 7-8, 2012.
32. VK. Ingle, JG. Proakis. Digital signal processing using MATLAB. Cengage Learning, 2012. pp.493-498.
33. de Chazal P, Heneghan C, Sheridan E, Reilly R, Nolan P, O'Malley M. Automated Processing of the single-lead electrocardiogram for the detection of obstructive sleep apnoea. *IEEE Trans Biomed Eng.* 2003;50(6):686-96.
34. JC. Principe, NR. Euliano, WC. Lefebvre. Neural and adaptive systems, Fundamentals through simulations. John Wiley & Sons, 2000.
35. Delorme A, Makeig S. EEGLAB Wikitorial. Available: <http://sccn.ucsd.edu/eeglab/>, 2011. (Adapted from: Delorme A, Makeig S. EEGLAB: an open source toolbox for analysis of single-trial EEG dynamics. *J Neurosci Methods*. 2004;134(1):9-21).
36. Bell AJ, Sejnowski TJ. An information-maximization approach to blind separation and blind deconvolution. *Neural Comput.* 1995;7(6):1129-59.
37. Lee TW, Girolami M, Sejnowski TJ. ICA using an extended infomax algorithm for mixed subgaussian and supergaussian source. *Neural Comput.* 1999;11(2):417-41.
38. Delorme A, Sejnowski T, Makeig S. Enhanced detection of artifacts in EEG data using higher-order statistics and independent component analysis.

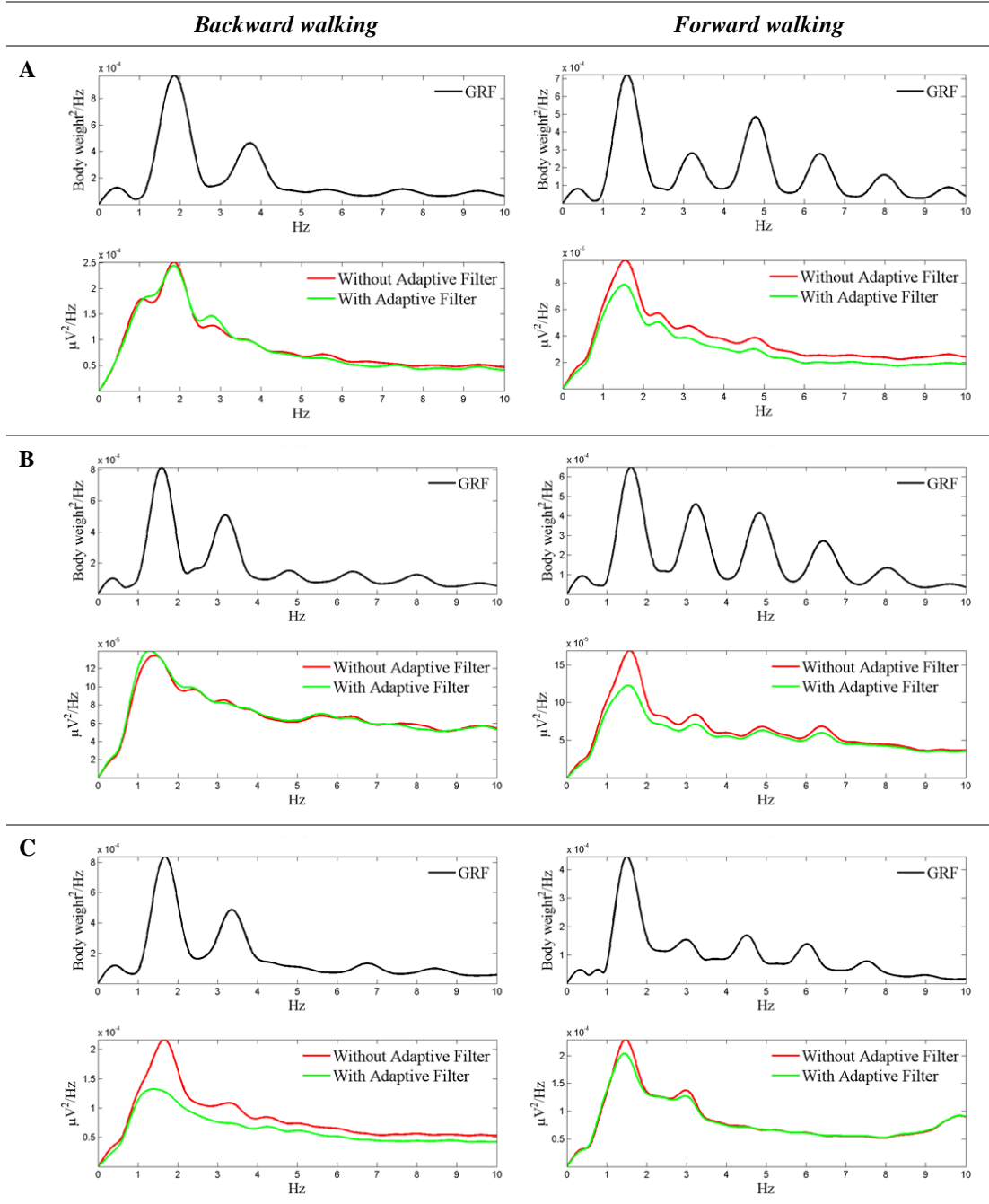
- Neuroimage. 2007;34(4):1443-9.
39. Buzsáki G, Mizuseki K. The log-dynamic brain: how skewed distributions affect network operations. *Nat Rev Neurosci*. 2014;15(4):264-78.
 40. Pivik RT, Broughton RJ, Coppola R, Davidson RJ, Fox N, Nuwer MR. Guidelines for the recording and quantitative analysis of electroencephalographic activity in research contexts. *Psychophysiology*. 1993;30(6):547-58.
 41. 張皓，2013，心電圖訊號波型的頻譜分析，碩士論文，國立中山大學機械與機電工程學系。
 42. Sterman MB. Physiological origins and functional correlates of EEG rhythmic activities: implications for self-regulation. *Biofeedback Self Regul*. 1996; 21(1):3-33.
 43. VB. Pavlenko, SV. Chernyi, DG. Goubkina. EEG correlates of anxiety and emotional stability in adult healthy subjects. *Neurophysiology*. 2009;41(5):337-345.
 44. Crabbe JB, Dishman RK. Brain electrocortical activity during and after exercise: A quantitative synthesis. *Psychophysiology*. 2004;41(4):563-74.
 45. Tanaka H, Monahan KD, Seals DR. Age-predicted maximal heart rate revisited, *J Am Coll Cardiol*. 2001 37(1):153-6.
 46. Grimshaw GM, Carmel D. An asymmetric inhibition model of hemispheric differences in emotional processing. *Front Psychol*. 2014;5:489.
 47. Hall EE, Ekkekakis P, Van Landuyt LM, Petruzzello SJ. Resting frontal asymmetry predicts self-selected walking speed but not affective responses to a short walk. *Res Q Exerc Sport*. 2000;71(1):74-9.
 48. Pfurtscheller G, Neuper C. Movement and ERD/ERS. The Bereitschaftspotential. 2003; pp.191-206.

49. Juri D. Kropotov. Quantitative EEG, Event-Related Potentials and Neurotherapy. Elsevier, 2009. pp.29-76.
50. Baumeister J, Reinecke K, Liesen H, Weiss M. Cortical activity of skilled performance in a complex sports related motor task. *Eur J Appl Physiol*. 2008;104(4):625-310.

Appendix

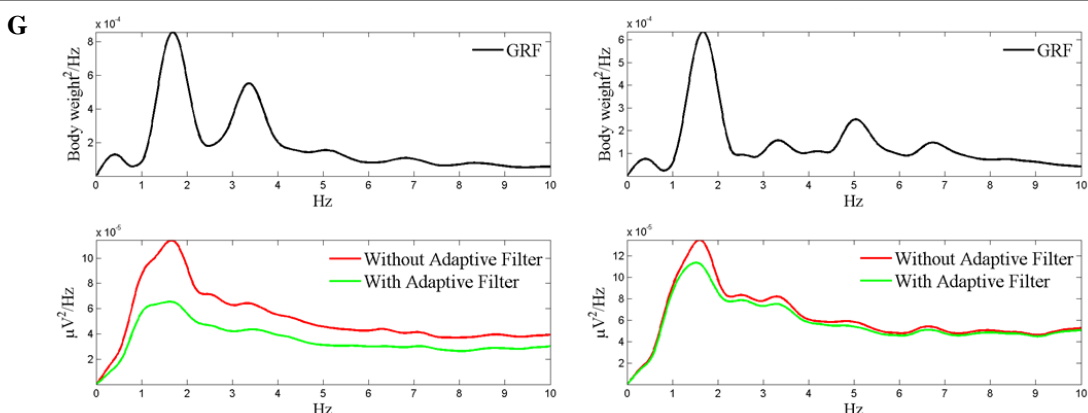
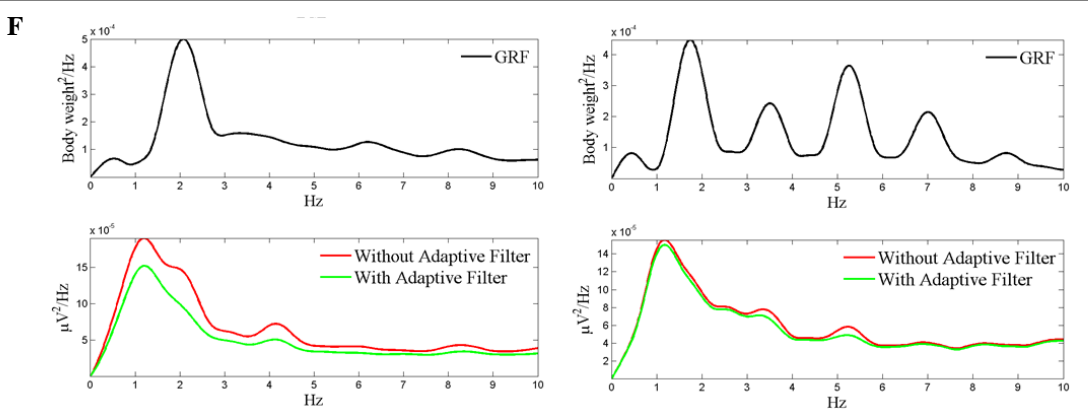
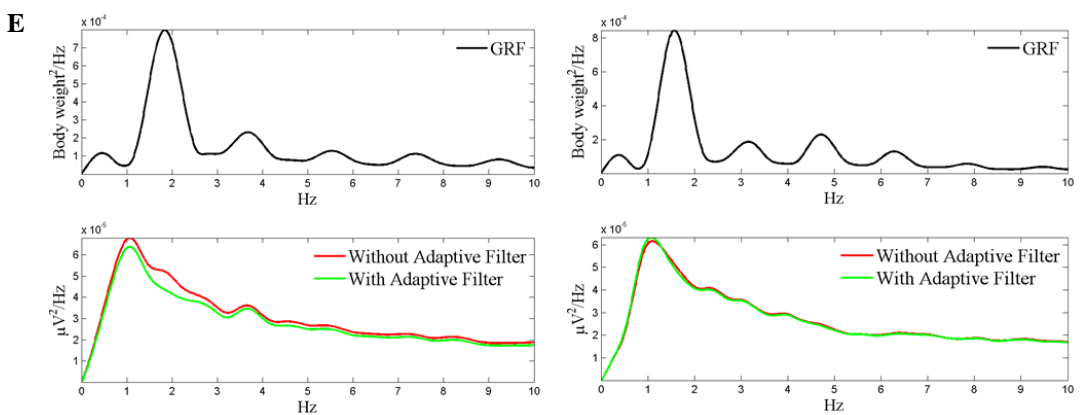
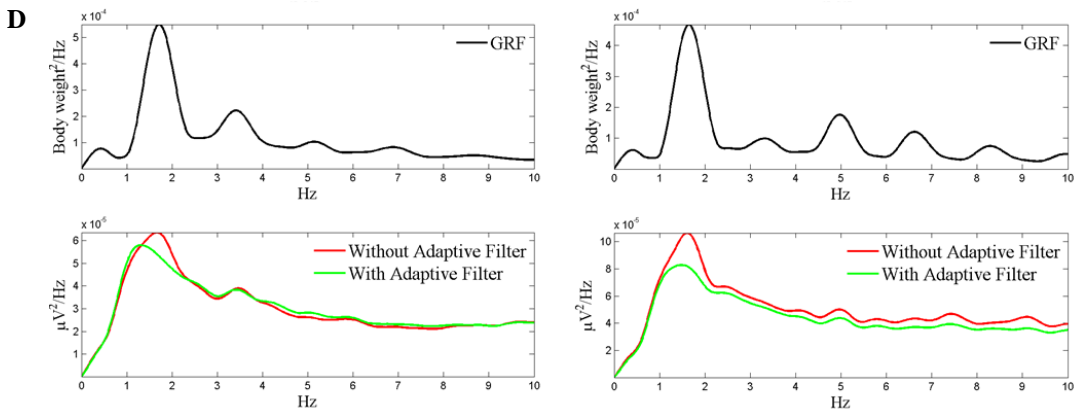
Appendix I. Gait-related Artifacts

- Ensemble channel-average PSD

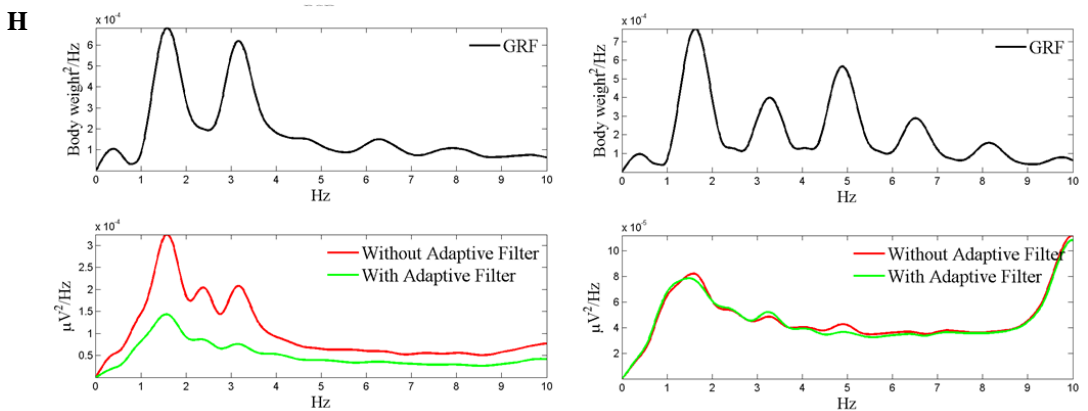


Backward walking

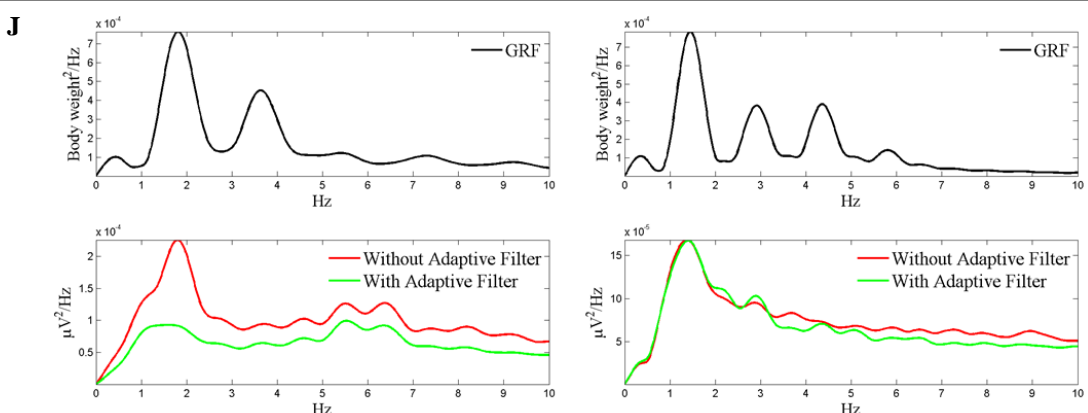
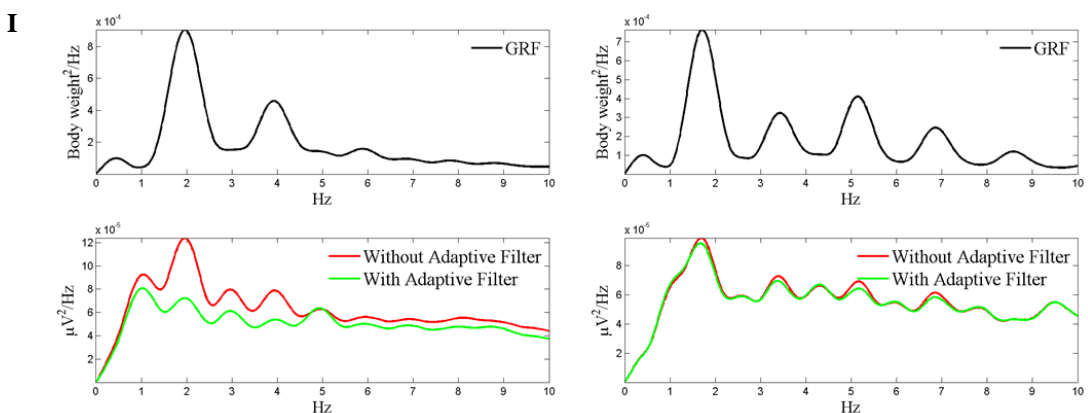
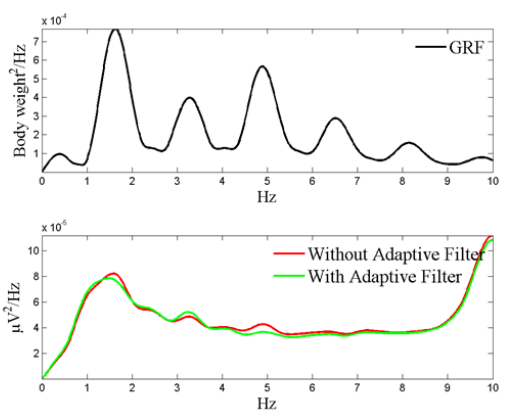
Forward walking



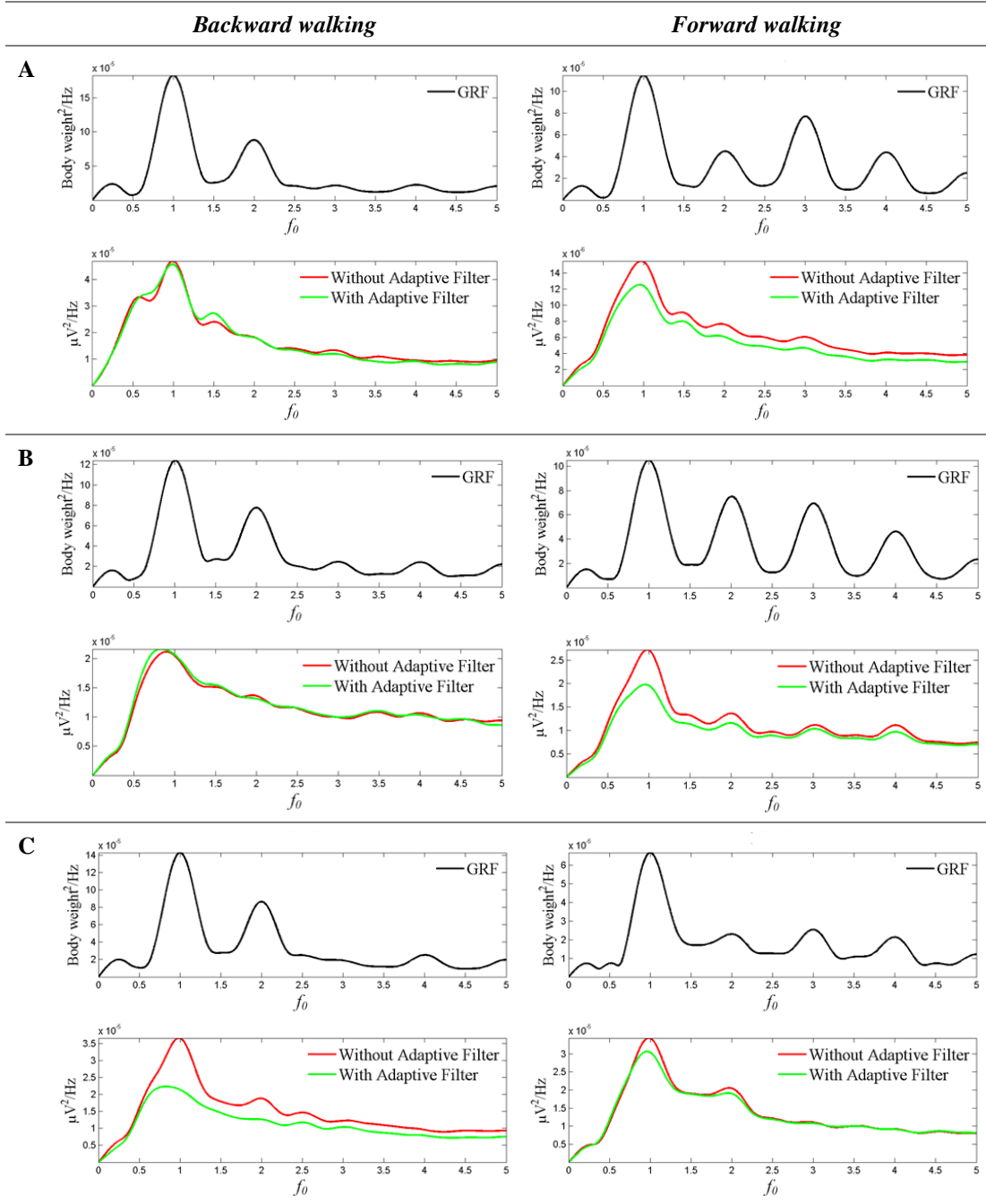
Backward walking



Forward walking



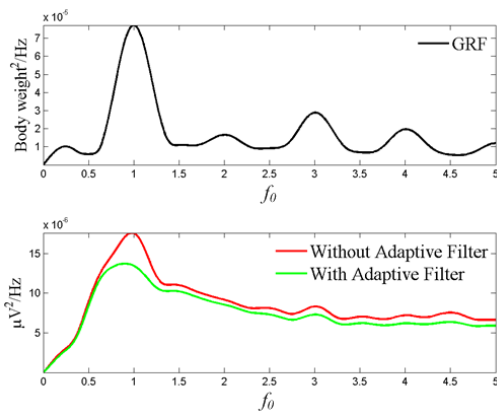
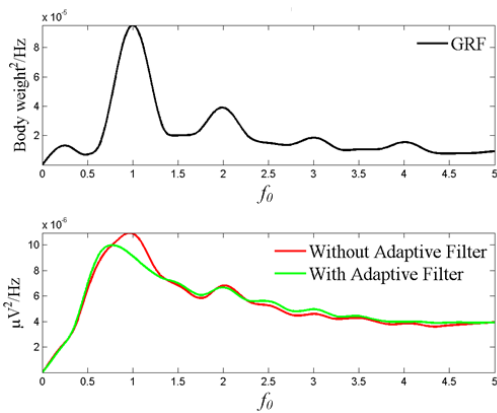
- Ensemble channel-average NPSD



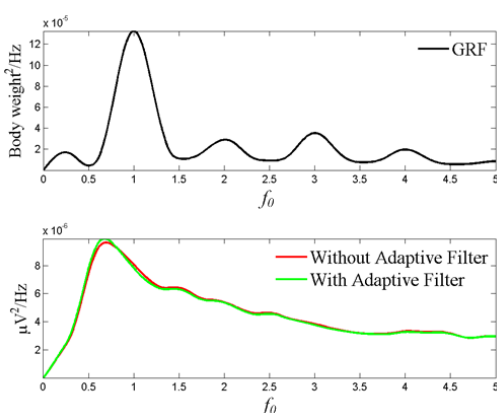
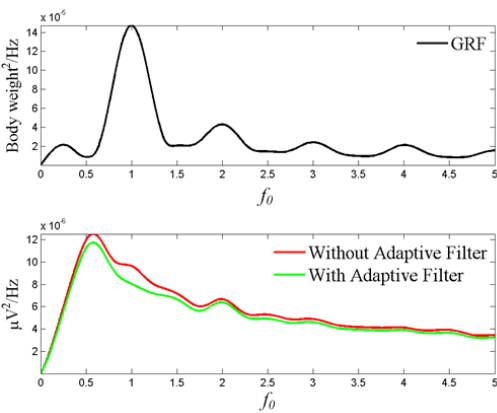
Backward walking

Forward walking

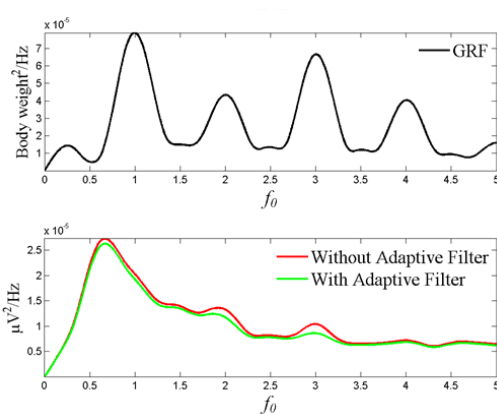
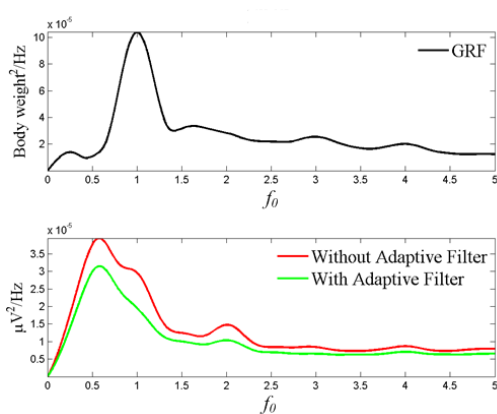
D



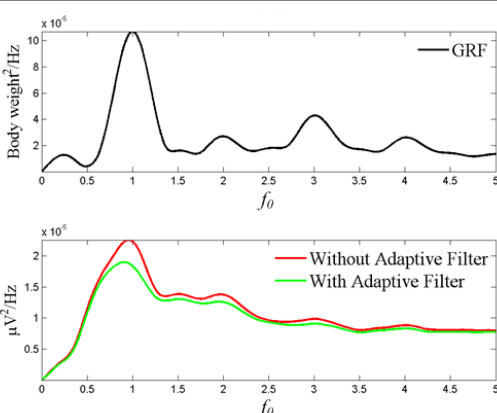
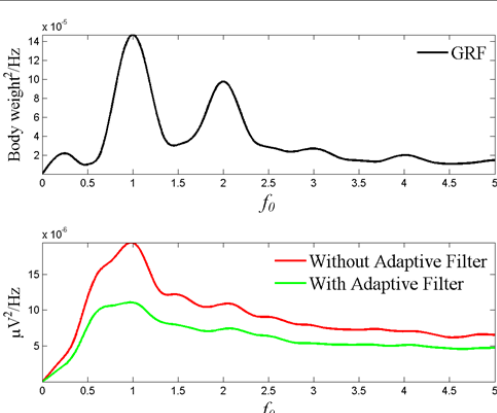
E



F

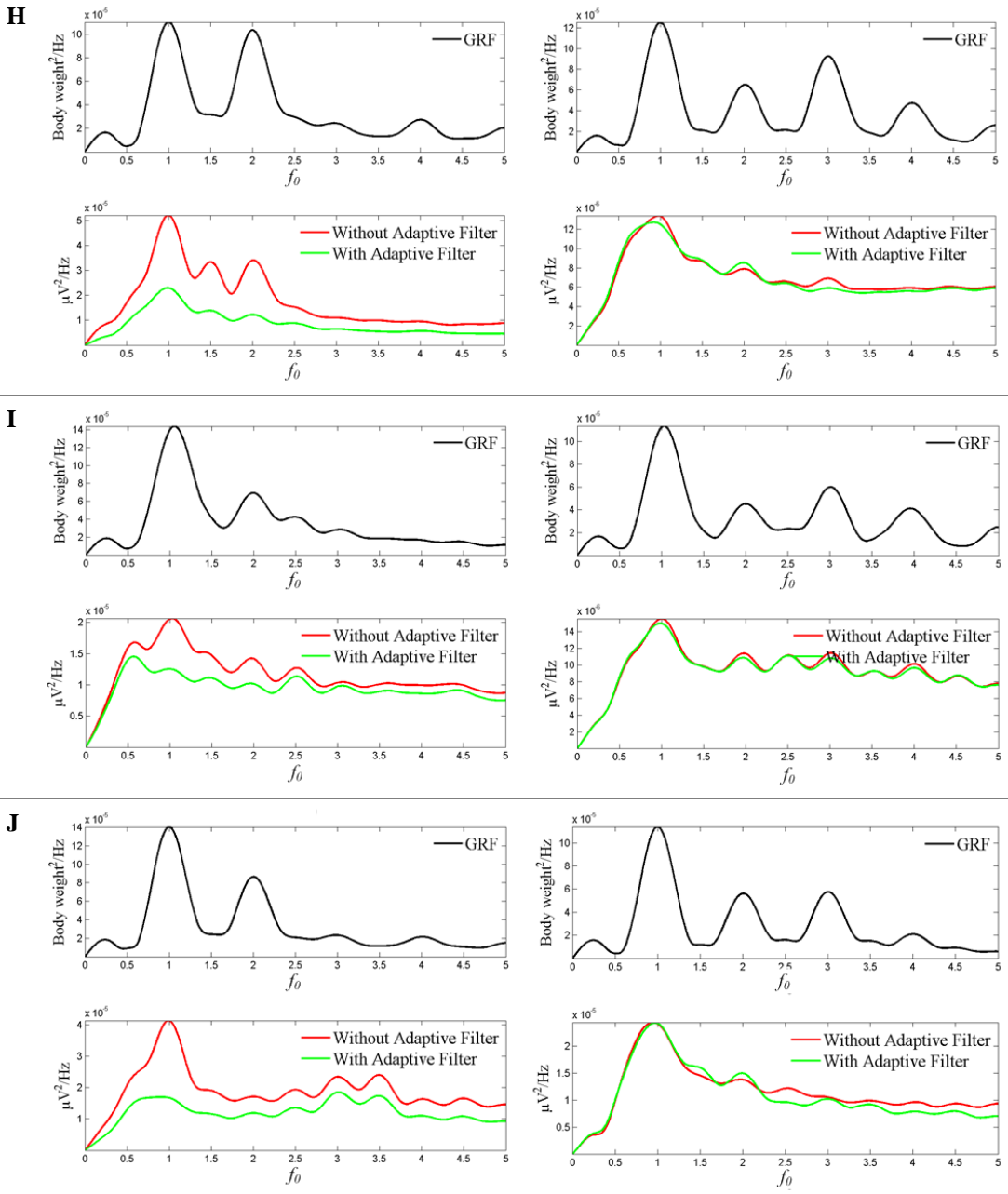


G



Backward walking

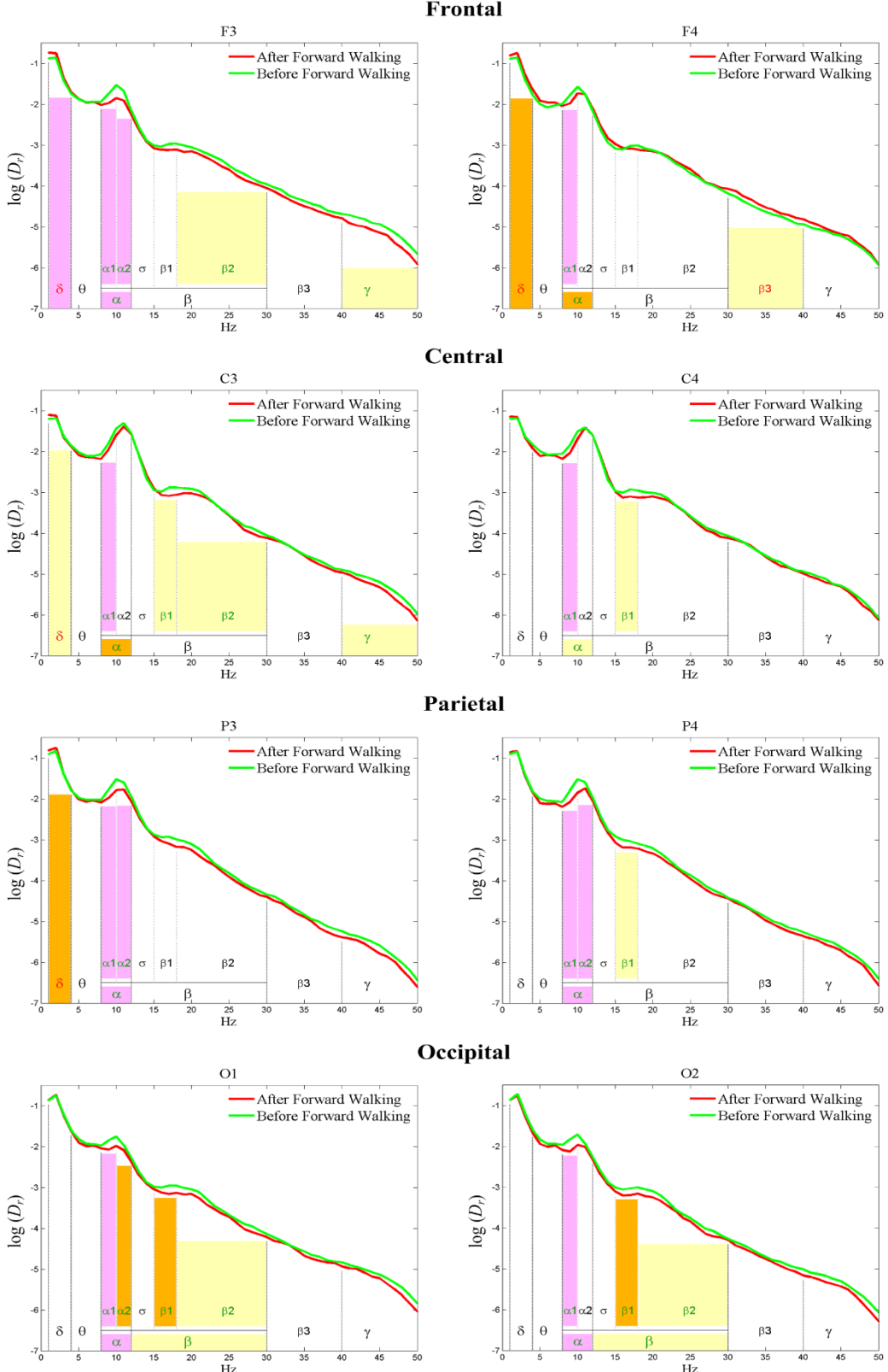
Forward walking



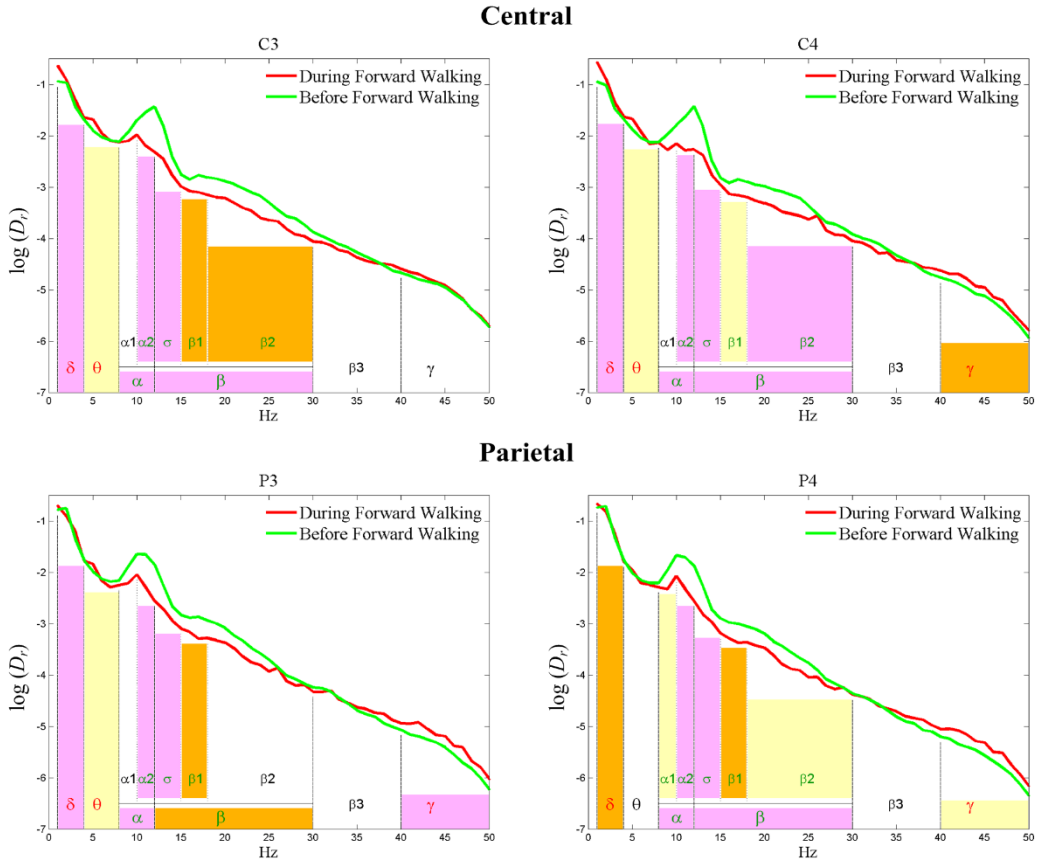
Appendix II. EEG Rhythms (Relative Power)

(1) Forward Walking

- *After versus Before Walking*



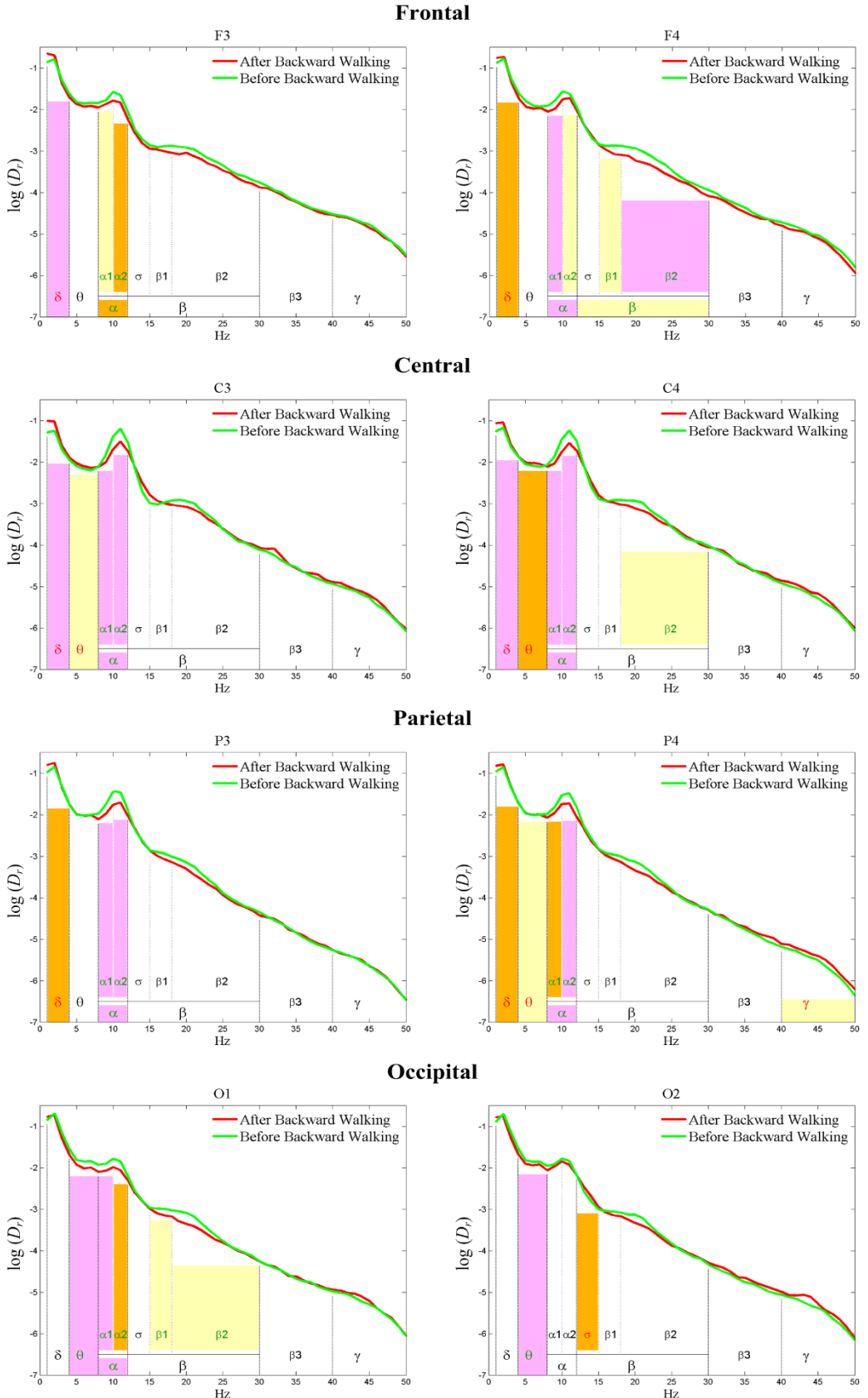
- *During versus Before Walking*



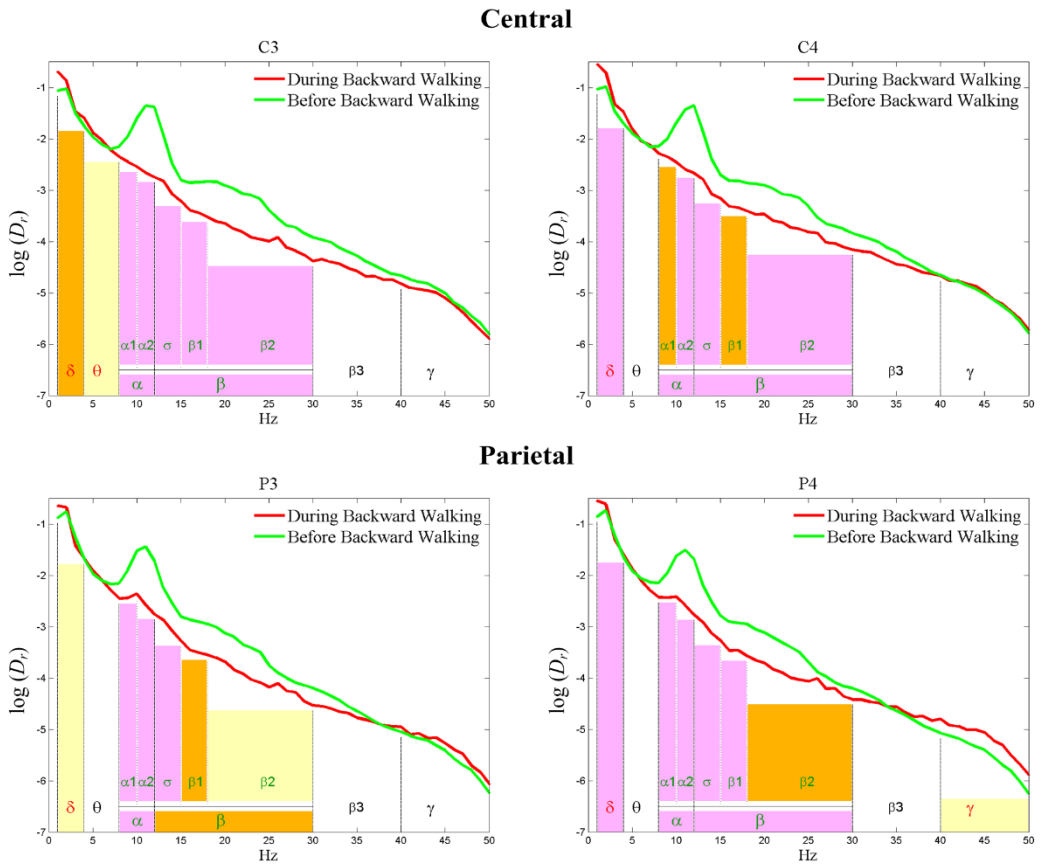
The area filled with purple, orange and yellow stood for p -value < 0.05 , $0.05 < p$ -value < 0.1 and $0.1 < p$ -value < 0.2 respectively. The colors of rhythmic labels represented the condition of larger rhythm power and the colors corresponded with the figure legend. For example, in “*Before versus During Walking*”, the green α rhythmic label in P4 indicated that the *Alpha* power showed a relatively large power before forward walking. This rule is suitable in Appendix II and Appendix III.

(2) Backward Walking

- After versus Before Walking

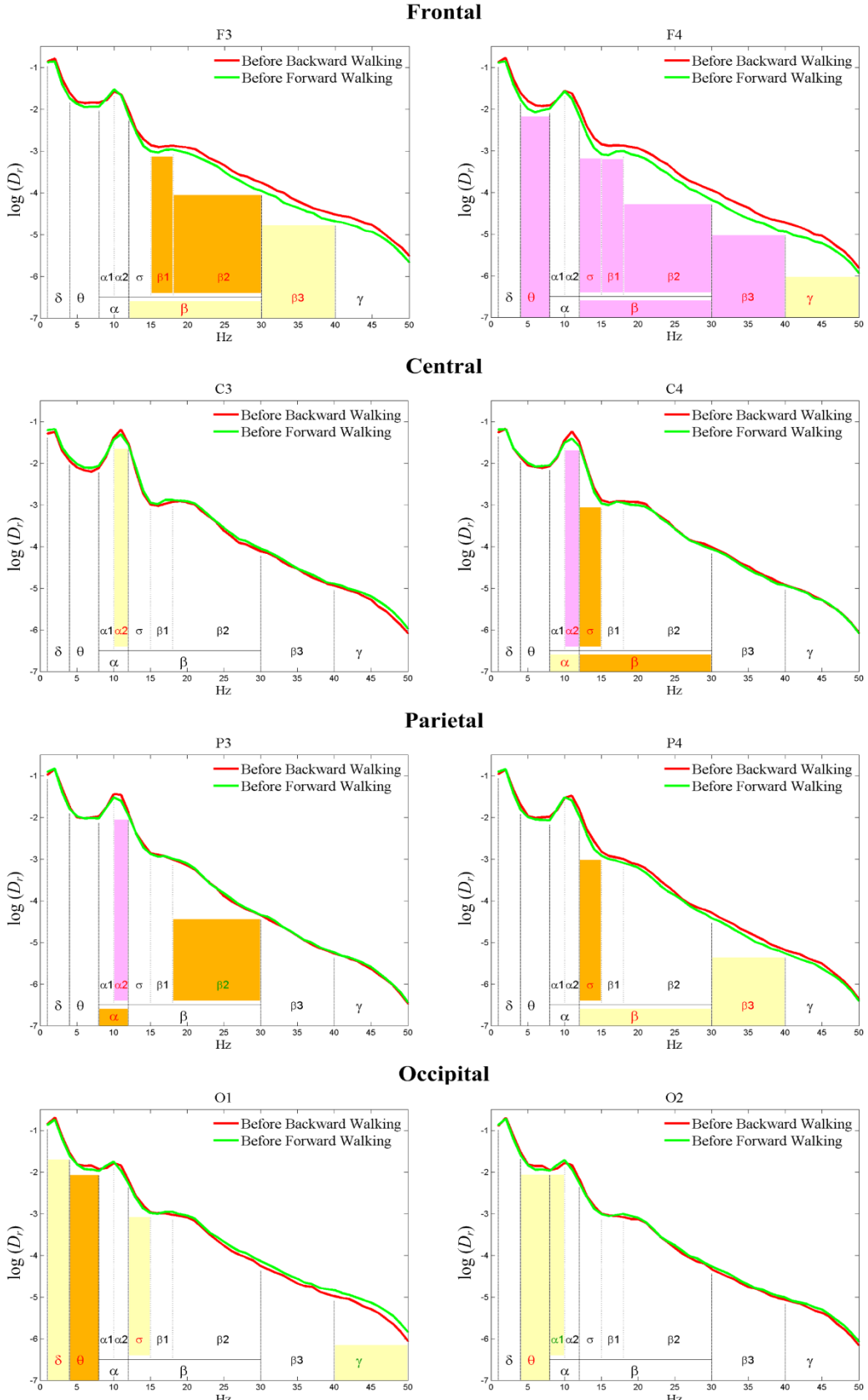


- *During versus Before Walking*

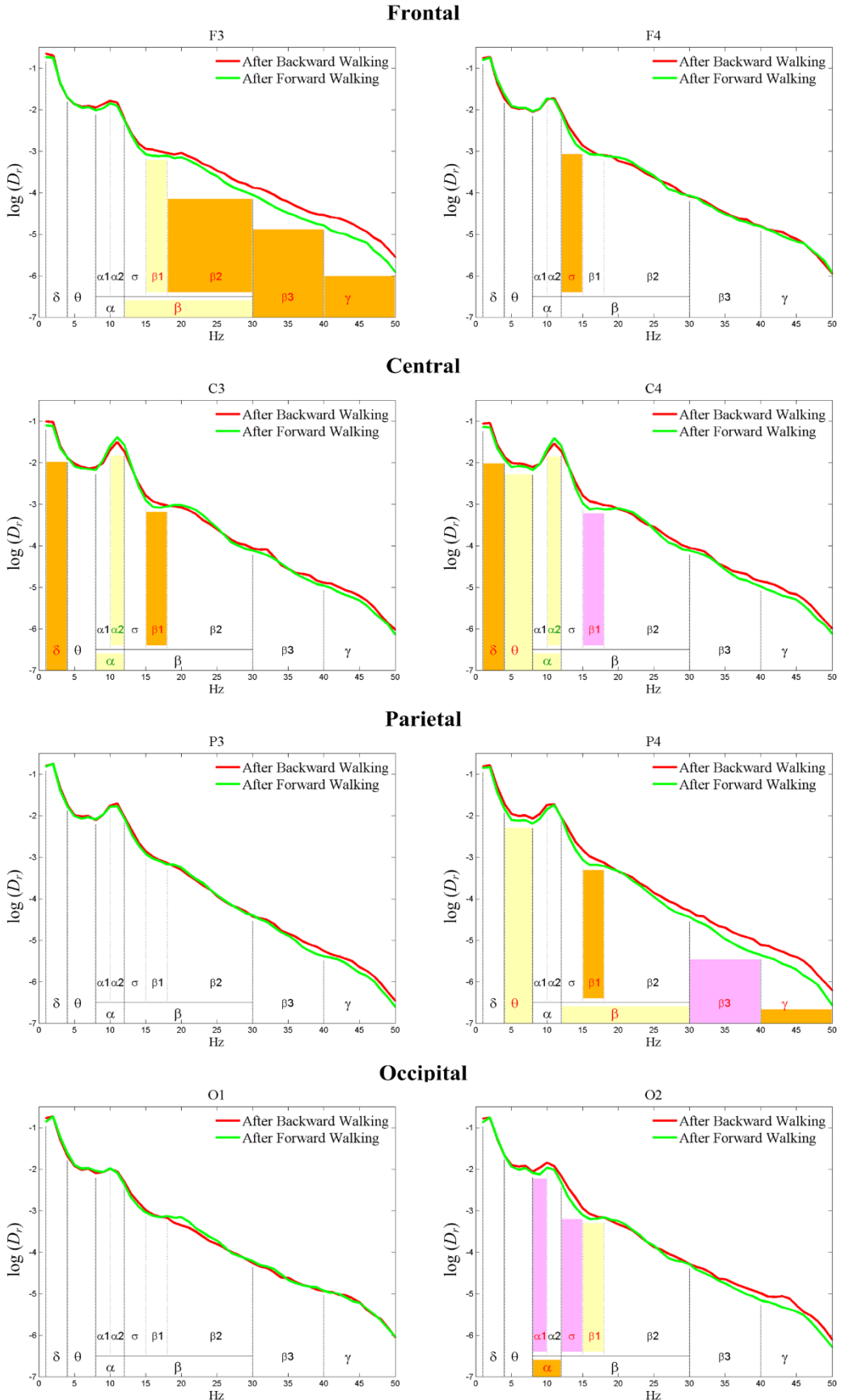


(3) Forward Walking versus Backward Walking

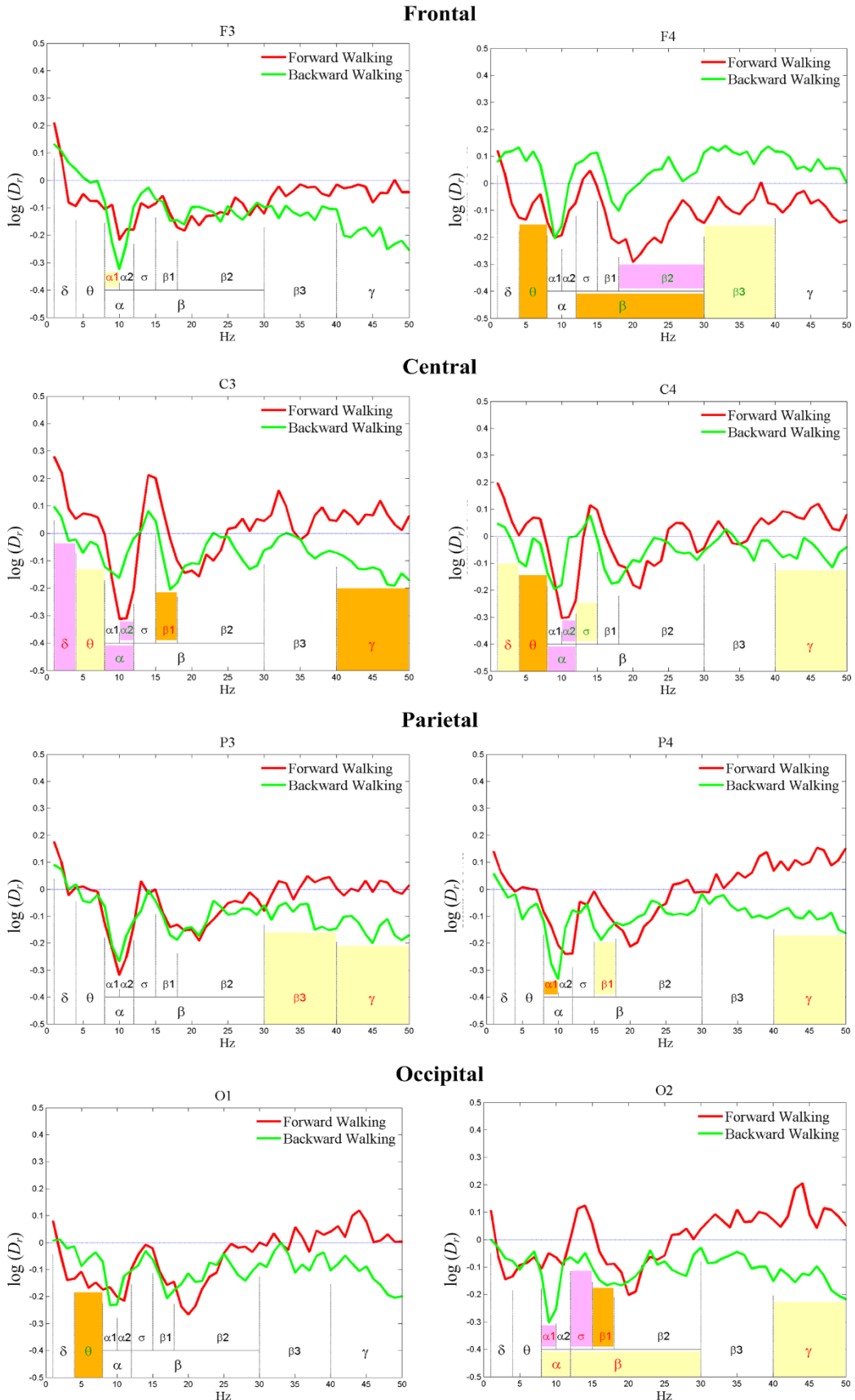
- *Before Walking*



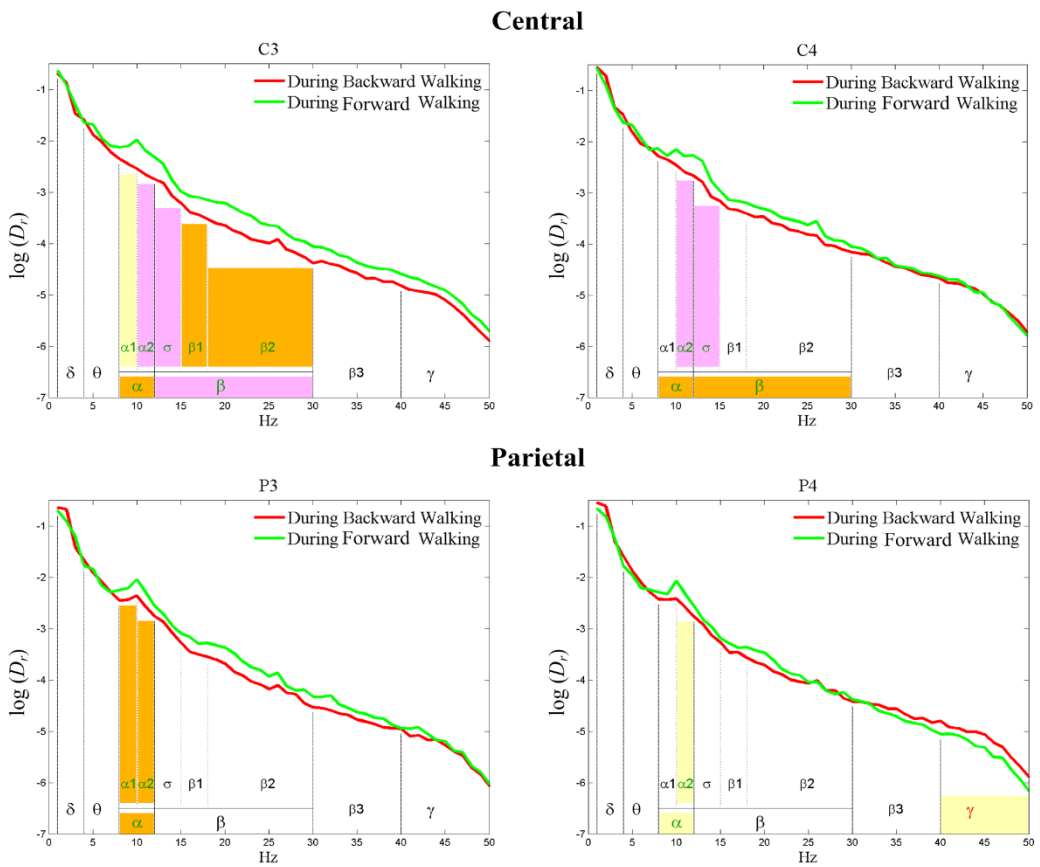
- *After Walking*



- *Rhythm Power Increment (After Walking)*

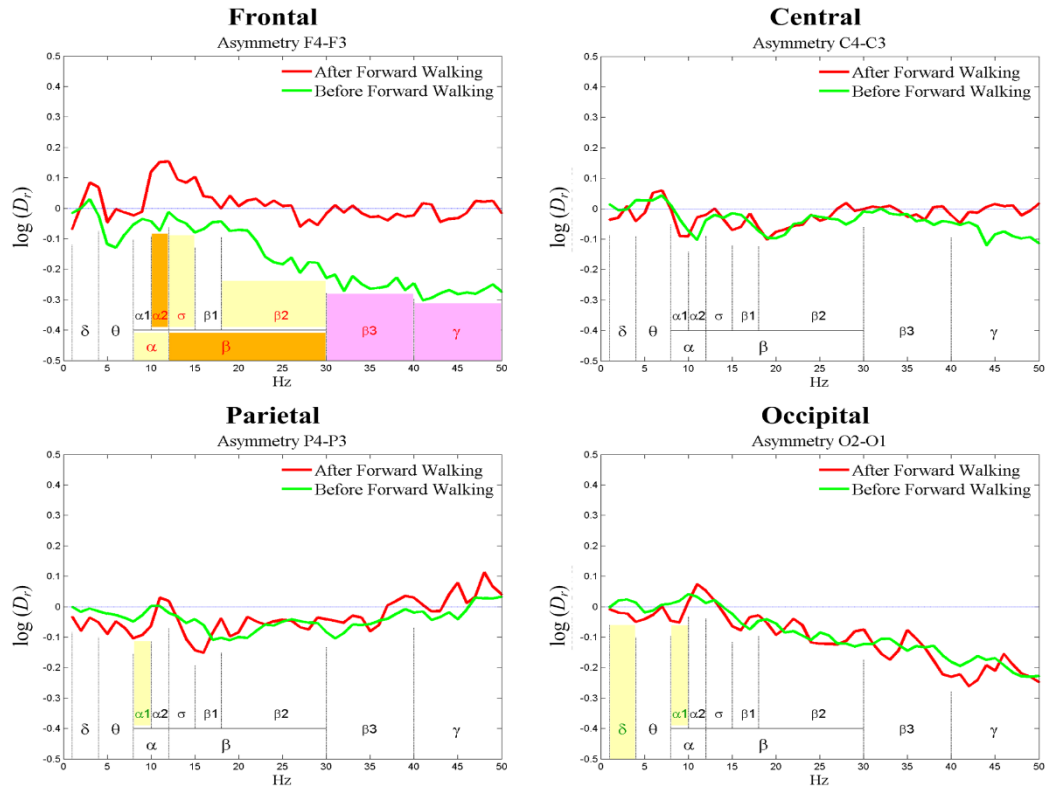


- *During Walking*

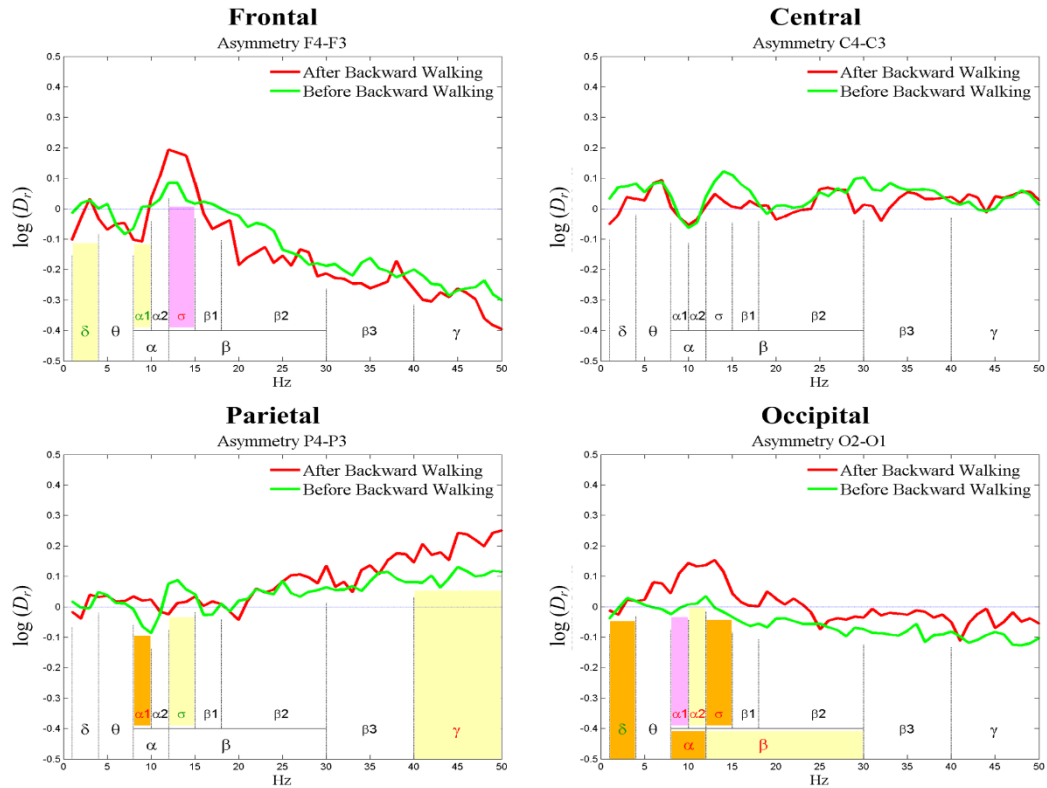


Appendix III. EEG Asymmetry (Relative Power)

(1) Forward Walking (*After versus Before*)

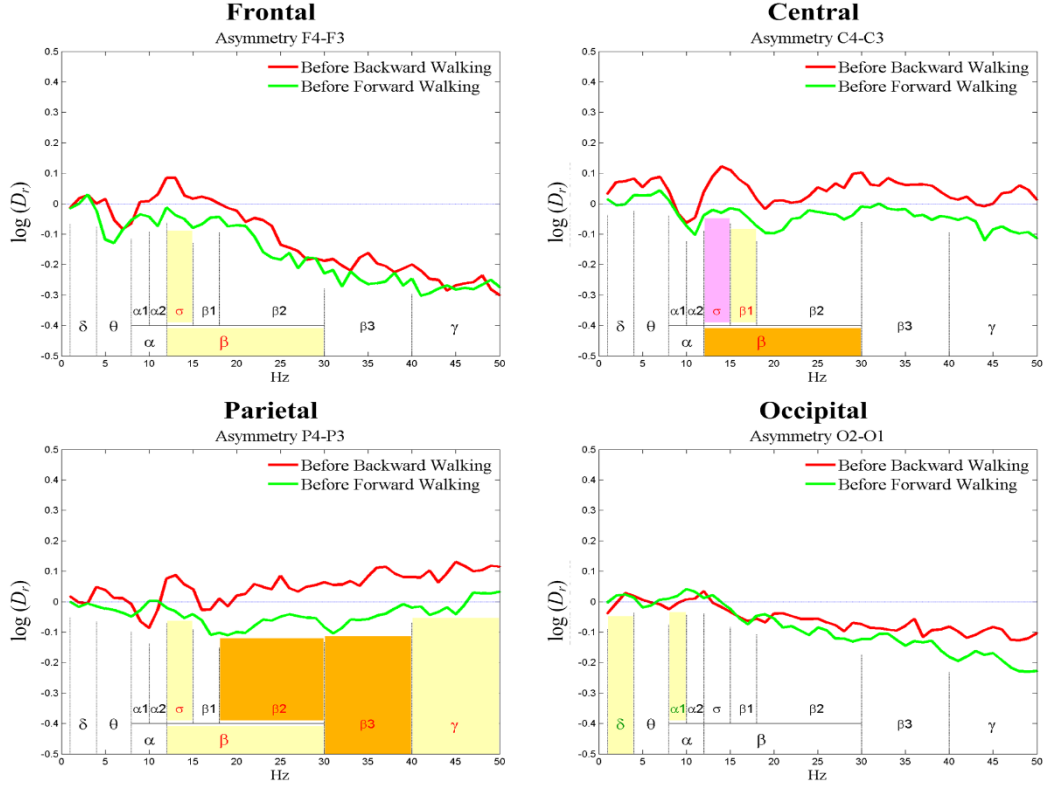


(2) Backward Walking (*After versus Before*)

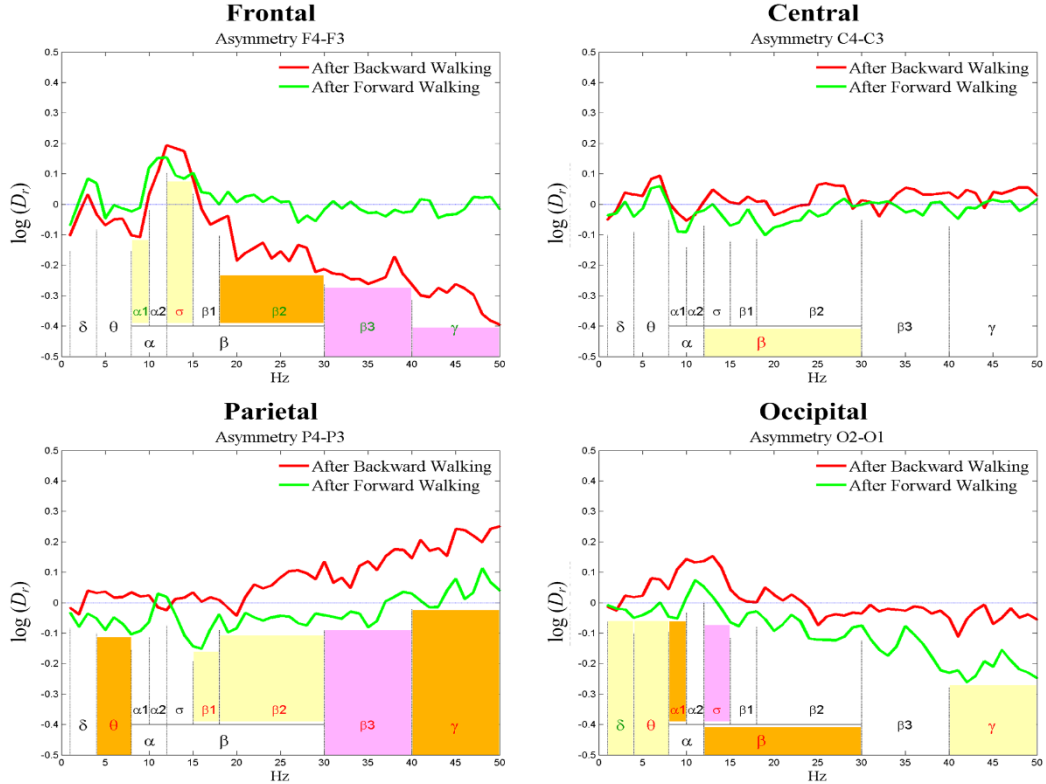


(3) Forward Walking versus Backward Walking

- *Before Walking*



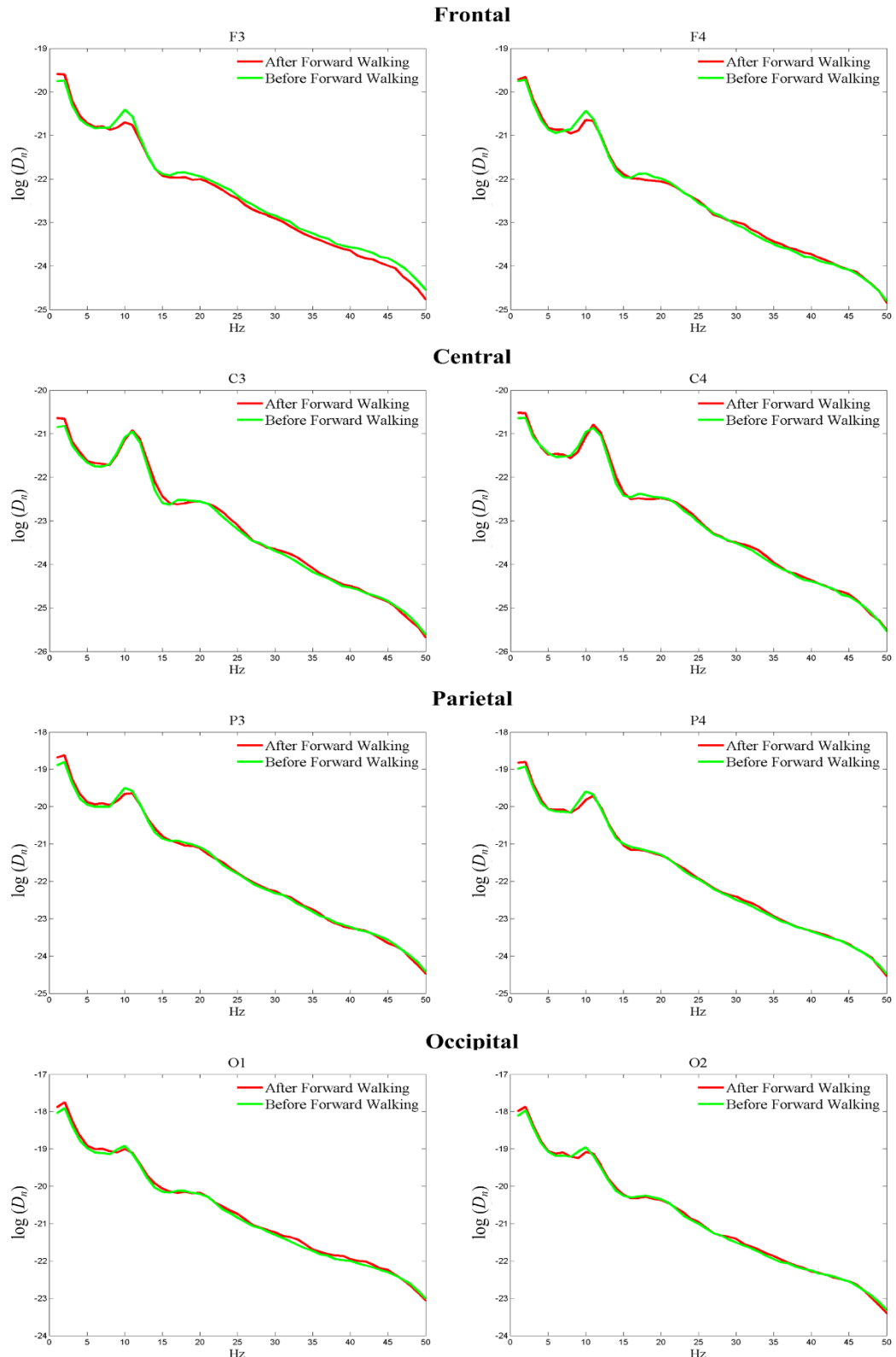
- *After Walking*



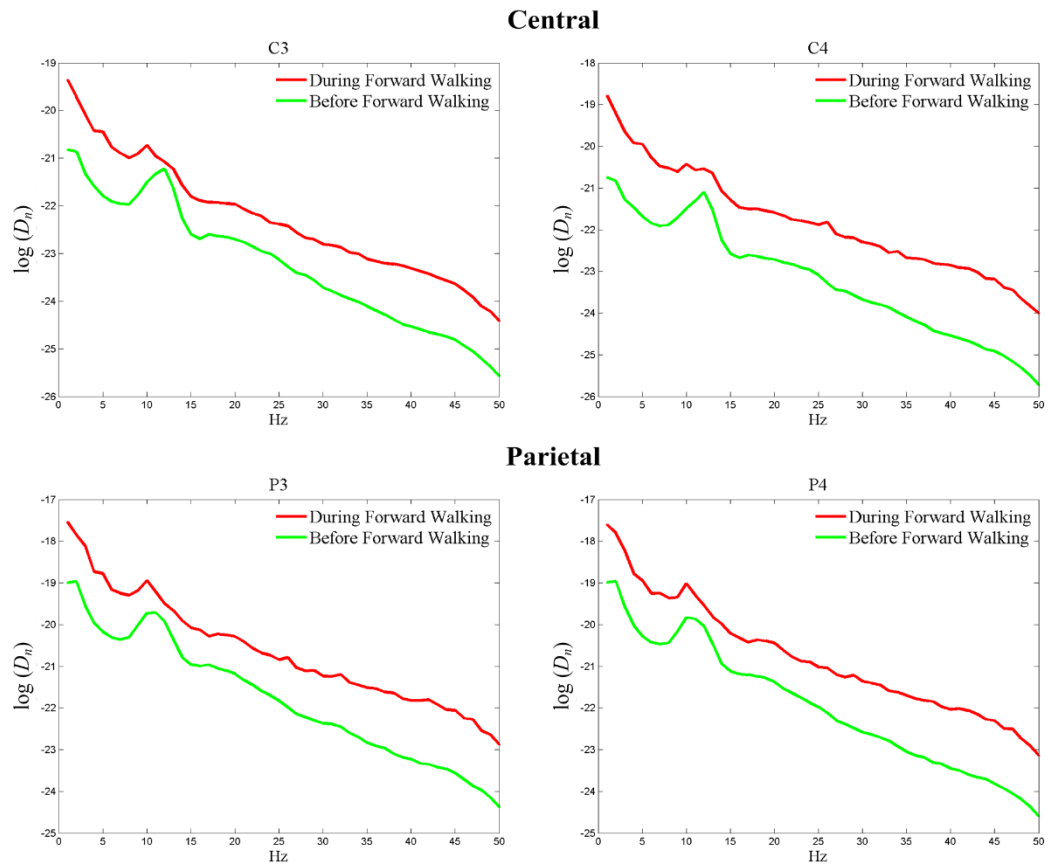
Appendix IV. EEG Amplitude Spectrum (Absolute Power)

(1) Forward Walking

- *Before versus After Walking*

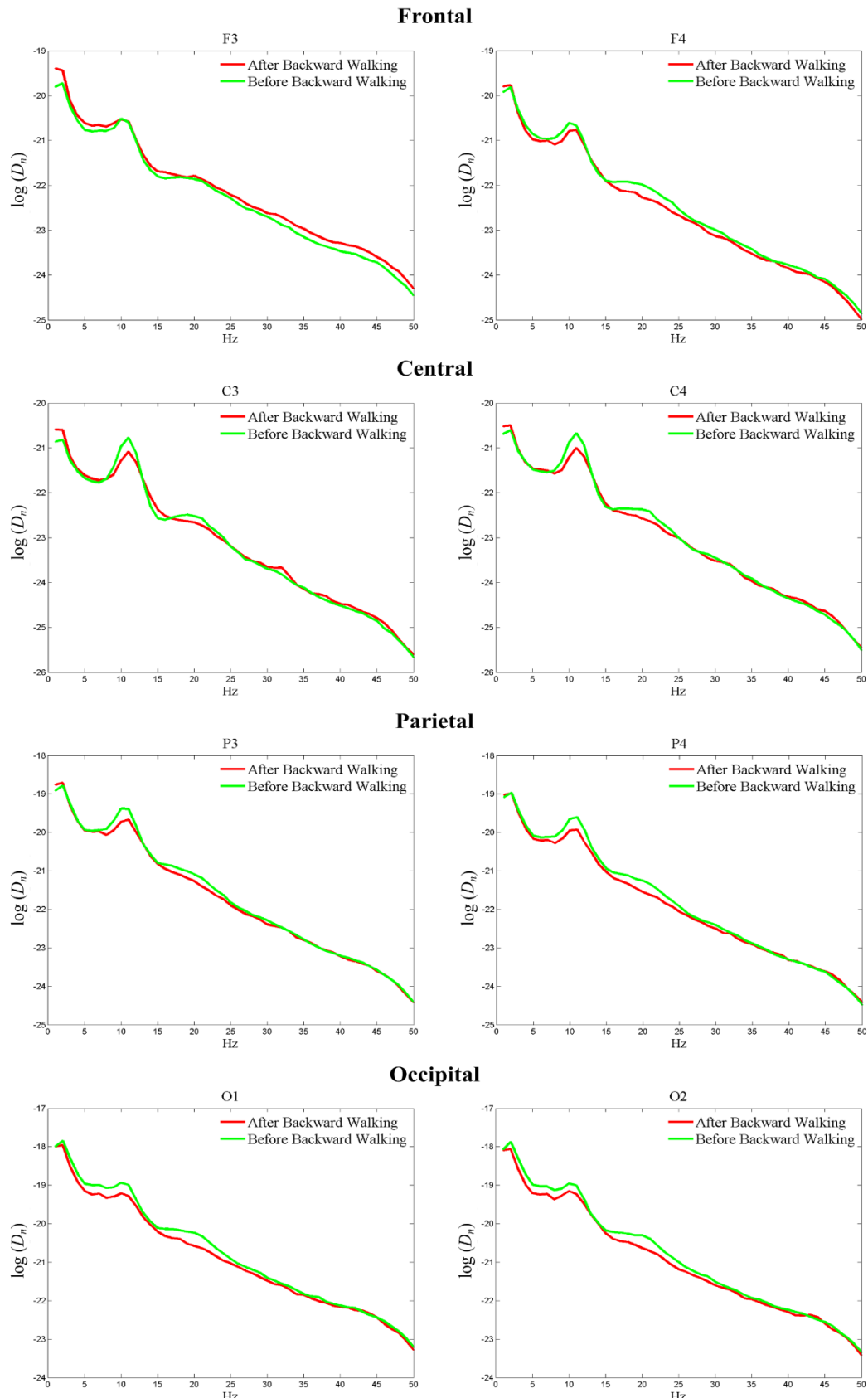


- *Before versus During Walking*



(2) Backward Walking

- *Before versus After Walking*



- Before versus During Walking

